universität wien

MASTERARBEIT / MASTER'S THESIS

Titel der Masterarbeit / Title of the Master's Thesis

„Simultaneous measurement of the spatial distribution of neurotransmitter target proteins in the rat brain using laser ablation inductively coupled plasma mass spectrometry“

verfasst von / submitted by

Christoph Wotawa, BSc

angestrebter akademischer Grad / in partial fulfilment of the requirements for the degree of

Master of Science (MSc)

Wien, 2021 / Vienna, 2021

Studienkennzahl lt. Studienblatt / degree programme code as it appears on the student record sheet:	UA 066 834
Studienrichtung lt. Studienblatt / degree programme as it appears on the student record sheet:	Masterstudium Molekulare Biologie
Betreut von / Supervisor:	Assoc.Prof.Priv.-Doz.Dr. Rupert Lanzenberger

Abstract

Introduction

Due to the role of up and down regulation of smaller and larger proteins in the brain in many psychiatric and neurological diseases, new technical developments in the last decades make it highly interesting to study the distribution of receptors and neurotransmitters. The exact distribution helps to understand different processes in disease development and their treatment, but in many techniques only one target can be measured at the same time and in staining application like immunohistochemistry many steps are needed to measure several targets.

Method

In this work the simultaneous detection of several proteins by means of antibodies was combined with the technique of laser ablation inductively coupled mass spectrometry (LA-ICP-MS) and the individual steps of tissue sample processing were optimized. For the simultaneous detection of certain serotonin receptors, specific antibodies were coupled with different isotopes of the lanthanides and 10 µm thick coronary cryosections of rat brains were incubated. The distribution was then measured by laser ablation inductively coupled mass spectrometry and displayed graphically with an imaging program.

Results

The distribution of two different receptors on coronary brain slices of adult rats on indium tin oxide coated glass cover slides was successfully measured at the same time. Isotope spiked gelatin standards could be established and used to quantify the Serotonin 5HT1A and 5HT2A receptor levels in different rat brain slices. The technologies of LA-ICP-MS and PET/MRI could be combined in the future by performing preoperative PET/MRI and postoperative processing, cutting and measuring of removed tissue by means of the method of LA-ICP-MS.

Conclusion

It could be shown that LA ICP MS is a powerful instrument for the simultaneous quantification of several protein targets. Even if the measurement time for an entire rat brain is time consuming, the advantage that over ten proteins can be measured at the same time clearly predominates.

Kurzfassung

Einführung

Durch die Rolle der Über- und Unterexpression kleinerer und größerer Proteine bei vielen psychiatrischen und neurologischen Erkrankungen sind neue technische Entwicklungen der letzten Jahrzehnte die Verteilung von Rezeptoren und Neurotransmittern sind von höchstem wissenschaftlichen Interesse. Die genaue Verteilung hilft, verschiedene Prozesse in der Krankheitsentwicklung und deren Behandlung zu verstehen, jedoch kann bei vielen Techniken nur ein Protein gleichzeitig detektiert werden, und in Färbeanwendungen, wie der Immunhistochemie, sind viele Schritte erforderlich, um mehrere Proteine zu messen.

Methode

In dieser Arbeit wurde der gleichzeitige Nachweis mehrerer Proteine durch Antikörpern mit der Technik der induktiv gekoppelten Massenspektrometrie und Laserablation kombiniert und die einzelnen Schritte der Probenverarbeitung optimiert. Zum gleichzeitigen Nachweis bestimmter Serotoninrezeptoren wurden spezifische Antikörper mit verschiedenen Isotopen der Lanthanoide gekoppelt und 10 µm dicke koronare Gefrierschnitte eines Rattenhirns inkubiert. Die Verteilung wurde dann durch induktiv gekoppelte Massenspektrometrie mit Laserablation gemessen und mit Bildgebungsprogrammen grafisch dargestellt.

Resultate

Die zeitgliche Messung der Verteilung zweier unterschiedlichen Rezeptoren in koronaren Hirnschnitten erwachsener Ratten auf mit Indium-Zinnoxid beschichteten Glasdeckgläsern konnte erfolgreich durchgeführt werden. Mit Isotopen versetzte Gelatine-Standards konnten erstellt und zur Quantifizierung der Serotonin 5HT1A- und 5HT2A-Rezeptorlevel verwendet werden. Die Technologien von LA-ICP-MS und PET/MRT könnten in Zukunft kombiniert werden, indem präoperatives PET/MRT und postoperative Prozessierung, Schneiden und Vermessen von entnommenem Gewebe mit der Methode der LA-ICP-MS durchgeführt werden.

Konklusion

Es konnte gezeigt werden, dass die induktiv gekoppelte Massenspektrometrie mit Laserablation ein leistungsfähiges Instrument zur gleichzeitigen Detektierung mehrerer Proteine ist. Selbst wenn die Messzeit für ein gesamtes Rattenhirn zeitaufwändig ist, überwiegt eindeutig der Vorteil, dass über zehn Protein gleichzeitig gemessen werden können.

Index of Abbreviations

5-HT	5-Hydroxytryptamine, Serotonin
5-HT1A	5-HT_{1A} receptor
5-HT2A	5-HT_{2A} receptor
AB	Antibody
AG	Antigen
(c)CT	(cranial) computed tomography
ICP-MS	Inductively coupled plasma mass spectrometry
IgG	Immunoglobulin G
IHC	Immunohistochemistry
ISH	*In-Situ* Hybridisation
ITO	Indium tin oxide
LA	Laser ablation
LA-ICP-MS	Laser ablation inductively coupled mass spectrometry
MALDI	Matrix-assisted Laser Desorption/Ionization
MAO-A	Monoamine oxidases A
MDD	Major depressive disorder
MRI	Magnetic Resonance Imaging
NMDA	N-Methyl-D-Aspartate
NMDAR	N-Methyl-D-Aspartate receptor
PBS	phosphate-buffered saline
PET	Positron-emission tomography
PFA	Paraformaldehyde
ppb	Parts per billion
SAD	Seasonal affective disorder
SERT	Serotonin transporter
TBS	Tris-buffered saline

Acknowledgment

Firstly, I want to thank Assoc.Prof.Priv.-Doz.Dr. Rupert Lanzenberger, who gave me the opportunity to learn these exciting methods and whose work group I was allowed to work with.

I also want to thank Univ.Prof. Dipl.-Ing. Dr.techn. Andreas Limbeck and his PhD students for their professional support with technical problems and all their answers to my questions.

Furthermore, I owe thanks to the staff and students of the Neuroimaging Lab for continuously motivating and supporting me especially Matej Murgas regarding image rendering.

I would additionally like to thank bachelor student Nina Plischek for the work done together, my partner Katharina and my sister Vanessa for proofreading and everyone else who encouraged me in writing this thesis.

Index of Content

Introduction

In recent years, the field of applications of laser ablation inductively coupled mass spectrometry (LA-ICP-MS) has developed significantly. Beginning with inorganic analysis in industries and geology, it now continues to shift towards organic samples [1, 2]. The high spatial resolution and the ability to detect multiple isotopes simultaneously provide a simple method to analyze biological samples quickly and without complicated sample preparation.

A diverse application of LA-ICP-MS detection for the quantitative analysis of biological samples is currently hindered by the lack of matrix-matched internal standards and calibration standards for reproducible microelement imaging of biological samples [3]. In order to make LA-ICP-MS a useful tool for clinical diagnostics, it is necessary to establish a reliable internal standardization for correcting laser and ICP-MS fluctuations, as well as for compensating tissue layer thickness inhomogeneity. Internal standardization approaching for solid sample matrices are mostly limited to natural element occurrences. Due to the inhomogeneity of biological samples, the choices of internal standards are limited to those with known homogeneous distributions in the biological matrix.

Two further possible applications of internal standards are examined here in this work. On the one hand, indium tin oxide coated slides (ITO slides) known from MALDI [4], and on the other hand, gold vapor coated silica wafers, which meet the requirements of an internal standard [5, 6].

Many psychiatric disorders and neurological diseases, such as major depressive disorder and schizophrenia, are associated with significant changes of specific protein or neurotransmitter levels [7, 8]. These proteins and transmitters are often up or down regulated and can be detected as biomarkers for diseases or disease stages in tissue samples.

Currently, immunohistological *ex vivo* staining is most commonly used for the visualization of protein expressions as well as for their localization. In this method, antigens are detected directly or indirectly via their complementary antibodies [9].

In the field of clinical *in vivo* diagnostics, EEGs with high temporal resolution [10] or imaging methods, such as computed tomography (CT), magnetic resonance imaging (MRI), positron

emission tomography (PET) or combinations, are used. However, PET can only measure one specific target at a time [11, 12].

LA-ICP-MS gives research the opportunity to simultaneously image several targets in a single tissue sample, without needing several washing steps and re-incubations, as it has to be done for several targets in immunohistochemistry (IHC). These combined facts make LA-ICP-MS an extreme powerful and time saving research methodology to gain more knowledge about protein distribution in different types of tissue within various disorders.

Theoretical Background

Psychiatric disorders

Changes in neurotransmission in various psychiatric disorders has been investigated and these alterations are associated with changes in receptor densities. These alterations can be found as up or down regulations in receptors, transporters or enzymes. The most prominent examples to be named are psychotic disorders like schizophrenia [13, 14] or mood affecting disorders like major depressive disorder (MDD) [15, 16] frequently associated with alterations in the monoaminergic neurotransmitter systems.

One of these monoamine neurotransmitter is 5-Hydroxytryptamine (5-HT), also known as Serotonin. The origin of the projections of the serotonergic modulation system is the raphe nuclei in the midline of the brain stem, with their projections throughout the central nervous system. These raphe nuclei, together with other transmitter systems, are closely linked to the control of the circadian rhythm and the various stages of sleep, as well as the control of mood and emotional behaviors [17, 18].

In order to understand these complex interactions and relationships, it has always been an important aim to visualize these monoaminergic alterations. These alterations can be measured by *in vivo* positron emission tomography (PET). However, a comparison should be carried out using the other quantitative techniques as LA-ICP-MS.

In the next sunsections I will explain conventional detection methods as well as the absics of the method used in this work and how antibodies can be labelled and used for this method.

Antibodies & Immunohistochemistry

Antibodies are glycoproteins in the class of globulins. They are part of the humoral immune defense and are produced by antigen-stimulated B-lymphocytes – the plasma cells – to specifically bind viruses, bacteria and toxins and thereby render harmless.

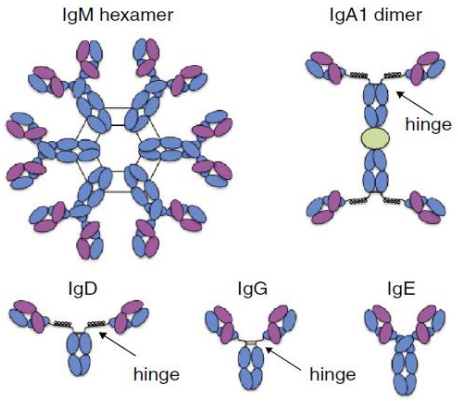

Figure 1: Diagram of antibody isotypes taken from a paper of R. J. Brezski published in 2016. Structures of immunoblobuline isotypes. IgM built after first contact with antigen. IgA common in mucosa. IgD most common and long lasting isotype. IgE protection against parasites and responsible for type 1 hypersensitivity [19].

As can be seen in figure 1, vertebrates have five distinct isotypes that have different conformations. Immunoglobulin G (IgG) is by far the largest antibody fraction in the blood plasma [19]. Among other things, antibodies are responsible for complement fixation and activation, opsonization of pathogens, and neutralization of toxins [20].

Antibodies consist of two variable antigen-binding regions, the Fab regions, and one constant regions (Fc regions). These Fab regions can bind pathogenic cells and microorganisms to allow them to be identified as foreign and destroyed. With these properties, antibodies act as mediators between antigens and immune defense mechanisms [20]. IgG occurs in the plasma as an Upsilon-shaped monomer. A monomer consists of two light and two heavy chains. One light chain consists of a variable and a constant unit, a heavy chain consists of a variable and, depending on the isotype, of three or four constant units. Resulting from these different composition possibilities, there is a high variability at the two ends of the antibody. This contact site consists of three short sections with significant amino acid sequence differences in the various regions. The high binding affinities in these areas are due to physical and chemical interactions. The hinge region between the two constant domains is responsible for the high spatial flexibility [19, 20].

With immunohistochemistry (IHC), scientists use the mentioned properties of the antibodies. This highly specific detection method is used for identification and histological localization of substances by means of specific antigen-antibody reaction [9]. The substance to be detected – usually peptides or proteins - acts as an antigen. The specific antibody (called primary antibody) is obtained from serum of an animal immunized with this substance (polyclonal antibody) or subsequently by hybridoma cells (monoclonal antibody) (Fig. 2). Hybridoma cells are produced by melding antigen-stimulated B lymphocytes, plasma cells, and an immortal cell line derived from a myeloma.

Secondary antibodies have to be directed against the animals' primary antibody. The principle of IHC is based on overlaying the tissue section with a diluted antibody solution and subsequent optical representation. Since the antibodies are not visible under the light microscope, two different strategies are used (Fig. 3). The first is the direct detection method in which the antibody is directly coupled with, for example, a fluorescent dye. The second variation is that in which the primary antibody recognizes and binds the antigen, a secondary antibody to which a fluorophore is bound, binds the primary antibody. Here, a detection reaction with an enzyme and a colored reaction product are used [9]. The last variant has the advantage of being more selective and that a further signal amplification effect occurs due to the second antibody.

Common fluorescent dyes used are: FITC (fluorescein isothiocyanate) giving a green color, TRITC (tetramethylrhodamine) giving an orange color or Alexa Flour dyes [22, 23], which can then be detected by fluorescence microscopy. Other detection methods for instance are based peroxidase or phosphatase reactions [9].

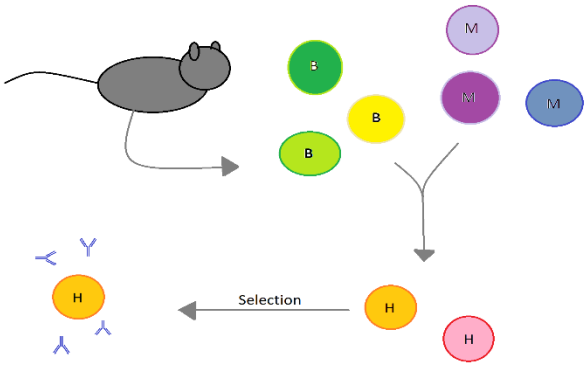

Figure 2: Scheme of monoclonal antibody production. Isolated B-lymphocytes (B) from spleen are fused with myeloma cells (M). Resulting indefinitely growing hybridoma cells (H) are selected and cultured by HAT medium (hypoxanthine, aminpterine, thymidine) and hybridoma cell producing the antibody with the highest affinity for the epitope of interest is further cultured and harvested [21]. Own figure.

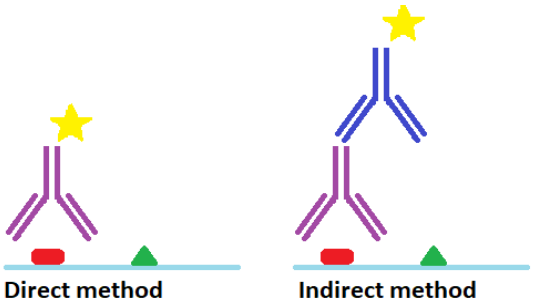

Figure 3: Detection strategies in IHC. Left: direct detection method - fluophore or reactant linked to primary antibody. Right: indirect detection method.- fluophore or reactant linked to secondary antibody. Own figure.

With these characteristics of the antibodies and the technical possibility of LA-ICP-MS to specifically detect multiple isotopes even in small quantities at the same time, it is a powerful method to combine antibodies with isotopes that rarely occur in animal tissue and thus to detect specific targets *ex vivo*.

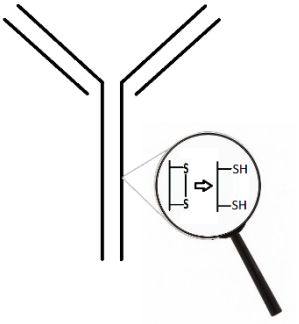

Figure 4: Scheme of disulfid bridge in de constant Fc region of an antibody. Disulfide bridges are possible sites for antibody labelling. Own figure.

One possible way to specifically label antibodies lies in the secondary and tertiary structure of the antibodies. Both variable and constant regions contains of several disulfide bridges that can be opened for the binding of further conjugates (Fig. 4). For this, Tris(2-carboxyethyl)phospin (TCEP) can be used as a reducing agent, but unlike other agents it has not to be removed for further applications as it does not contain sulfhydryl groups [24, 25]. The reducing property of TCEP makes it possible to selectively reduce disulfide bridges of the antibody and make them accessible for further modification. Commercially available kits with conjugates of carrier complexes and rare earth elements make it possible to combine these methods and use them for the detection of a wide variety of epitopes.

Autoradiography

Autoradiography is a method for the detection and localization of radioactive substances in histological specimens (Fig. 5). Target molecules are previously labeled with radioactive substances. For example, tritium 3H instead of protium 1H is incorporated into an amino acid. The radioactively labeled amino acid is then taken up to track the pathway of the amino acid in the cell and to better track the local and temporal course of protein biosynthesis. A photographic film is then coated on the preparation. This film is developed after a certain irradiation period.

The silver bromide crystals in the film act as microdetectors and are reduced to elemental silver by irradiation [26]. These silver grains can then be detected under the light microscope. Since the number of silver granules formed is proportional to the radioactivity, quantitative data can also be given.

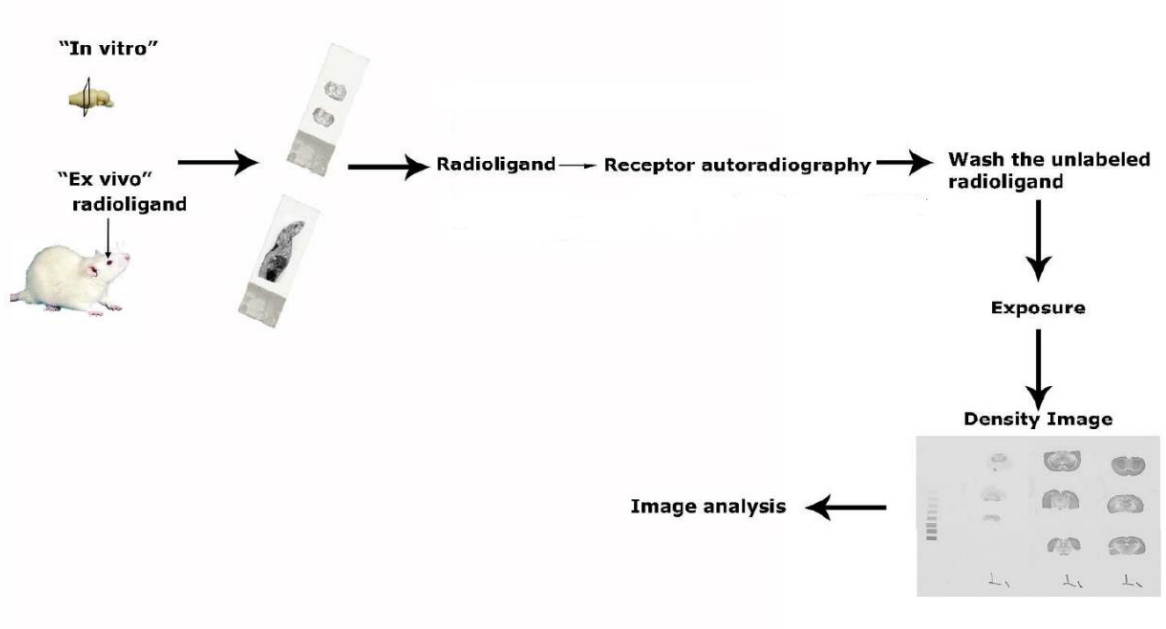

Figure 5: Diagram of autoradiography procedure taken and adapted from a paper of I. Manuel from 2015. Sample is incubated and then covered with x-ray film or nuclear emulsion plate [27].

Laser Ablation

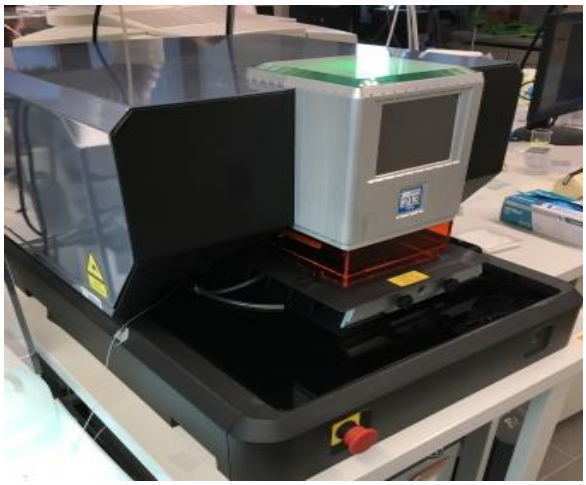

Figure 6: NWR213 Laser ablation system. Core unit is a Nd:YAG laser, that makes it possible to scan solid samples. Own figure.

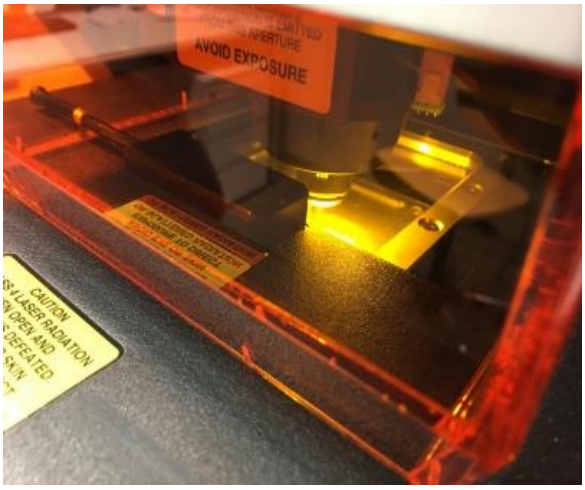

Figure 7: Laser ablation chamber. Specimen fixed on glass slide is ablated to aerosol and transported to ICP-MS by helium carrier gas. Own figure.

The tool used in this study is the NWR213 Laser Ablation System by Elemental Scientific Lasers (ESI), (Bozeman, Montana, USA; http://www.nwrlasers.com/), shown in figure 6 and 7. It consists of an Nd:YAG (neodymium-doped yttrium aluminium garnet) laser firing in a Wavelength of 213 nm and a maximum repetition rate of 20 Hz. The maximum fluence of the laser is about 25 J/cm^2 at the sample surface and the laser spot size is variable between 4 - 250 µm [28].

The Nd:YAG laser is one of the most widely used solid state lasers, which, in addition to being used in the laser ablation of biological and geological samples, is also used in medicine for performing endoscopic and surgical procedures [29].

The core of the laser is an artificially produced crystal with a regular structure, the yttrium aluminum garnet (YAG), which has been enriched with an average of 1.5% neodymium atoms [30]. The crystal is made by the Czochralski method. Here, all components of the manted crystal are melted together in a melting pot. A seed crystal on a metal rod of the crystal to be grown is lightly dipped into the melt. At the right temperature, the crystal now crystallizes on the seed crystal and the crystal can be pulled out by slowly lifting the seed crystal out [31].

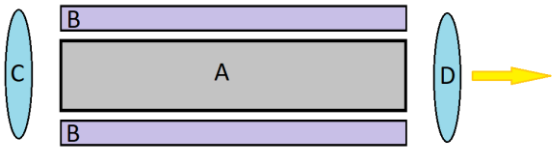

Figure 8: Scheme of Nd:YAG Laser setup. A: Nd:YAG crystal as the core oft he optical resonator. B: Laser diods or flashtubes exciting the electrones of Neodymium. C: Totally reflecting mirror. D: Semitransperent mirror that can reflect and release the laser beam. Own figure.

The electrons of neodymium in the crystal are excited by optical pumping of laser diodes or flashtubes. The totally reflective and semi-reflective mirrors form an optical resonator with the crystal, which emits infrared light with a wavelength of 1064 nm. A schematic representation of the laser can be seen in figure 8. Since UV light leads to better sample removal during laser ablation, the lights wavelength is changed to 213 nm by a fivefold frequency multiplication [32]. The laser beam is directed into the ablation chamber, passes through the “cap” and penetrates the sample on the movable sample table (Fig. 7 & 14). The cap is cylindrical and open at the top and bottom. From this cap, the aerosol created by the ablation is transported directly to the ICP-MS by the carrier gas helium. The cap also enables small samples or areas to be measured with as little aerosol loss as possible [33].

The Laser Ablation System is connected to a ESI New Wave Research distilled water cooling system.

Inductively coupled plasma mass spectrometry

Inductively coupled plasma mass spectrometry is an analyzing method used in simultaneous elemental analysis. This method was originally developed for the analysis of liquid samples. A peristaltic pump conveys the solution to be examined to a nebulizer, from which the aerosol produced, is conveyed to the ICP-MS. With this method, e.g. trace elements and the slightest heavy metal contaminations in µg per Liter range can be detected.

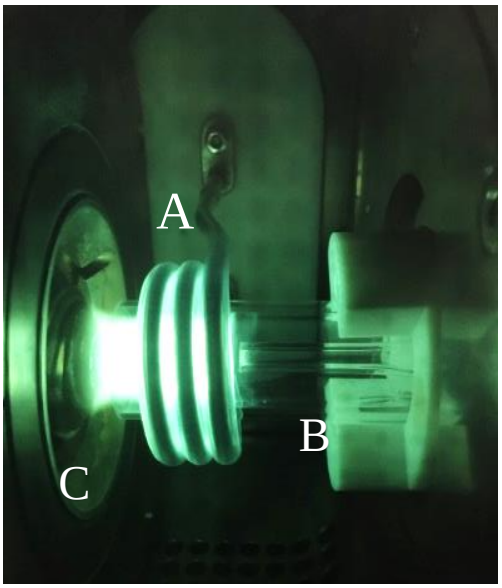

Figure 9: Switched on torch with green Argon plasma. A: Coil for microwave field. B: quartz tube. A and B together build the plasma torch. C: Sample cone. Own figure.

The central component therefore is the quartz torch consisting of three cylindrical layers. The carrier gas with the aerosol flows through the innermost tube. Cooling gas flows in the middle layer and the gas that generates the plasma flows in the outermost layer. Usually argon is used here in all three cases. The end of the quartz torch is wrapped in a cooled coil (Fig. 9). A generator conducts high frequency to this coil, creating a microwave field with a strength of 750 - 1500W [34, 35]. The argon passed through the torch couples with the microwaves and brings the gas into the most energetic of the four physical states - the plasma (Fig. 9). A schematic image of the setting can be seen in figure 10, found in the operating manual of the used ICP-MS unit. In the argon plasma the introduced sample aerosol is heated up to 10,000 K, whereby it is atomized and ionized. In the subsequent interface, the sample is drawn into a chamber with normal pressure via the sampler cone (visible on the left side in figure 9, C) into an area with negative pressure (0.002 bar) [35]. The sample is then further drawn into the high vacuum chamber through the skimmer cone.

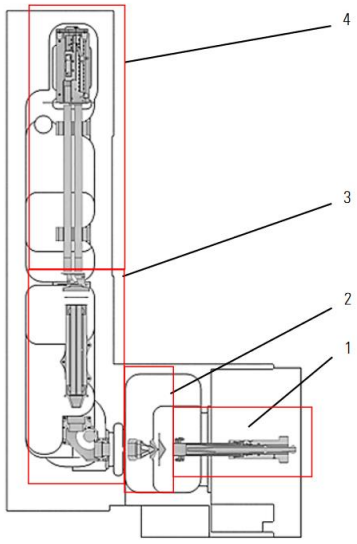

Figure 10: Schematic front view of the ICP-MS unit. 1: Sample introduction. 2: Interface. 3: Ion optics. 4: Mass analyzer. Image from Thermo Scientific.iCAP-Q Operating Manual [65] .

The ion optic then ensures that the gas cloud, which spreads diffusely in a vacuum, is directed to the detector as a thin beam. It is a metal cylinder to which electrical voltage is applied to prevent particulates, neutral species, and photons from reaching the detector by electrostatically bending the ions by 90° into the mass analyser [35].
The quadrupole technique is built in the device, which is used for this work, and thus represents the most compact mass spectrometer. Two mutually independent electrical voltages are applied to four parallel and symmetrically aligned metal rods. DC voltage is applied to all four, which leads to four concentric electromagnetic fields. A rotating high frequency is also applied alternately to two opposing metal rods. The resulting AC/DC ratio of the fields now create a spiral path that filters out ions and only sends ions of a certain m/z ration in a stable trajectory to the secondary electron multiplier (SEM) detector [35]. Here in this SEM, the ions are converted into electrical signals and amplified. An incoming ion is directed to an electrode called a dynode, where it releases an electron. This electron is then passed through an electric field to a second dynode, where two electrons are released. If this process is repeated a few times, the smallest signals from individual ions can be significantly amplified and detected with high temporal resolution (Fig. 11).

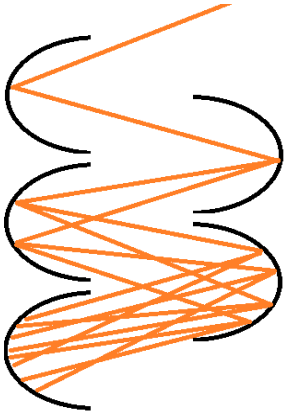

Figure 11: Scheme of secondary electron muliplier (SEM). Incomming ion releases one electron at first dynode. This electron releases two secondary electrons at the second dynode and so on. Own figure.

The ICP-MS unit used in this study is iCAP Q from Thermo Scientific coupled to an external water cooler.

LA-ICP-MS

The LA-ICP-MS is a high-resolution method for rapid multi-element analysis of solid sample materials. Originally developed for geological and material-analytical approaches [2, 36], it also offers many potential uses in biological or medical studies [37, 38]. This method can make a significant contribution to the distribution of elements in biological tissue or the pharmacokinetics of drugs such as chemotherapeutic drugs [39]. In order to combine both methods of laser ablation and the ICP-MS for bio imaging in a meaningful way, it is necessary to let both devices work synchronously. The program for controlling and measuring the element distributions does not start the detection until the laser control program forwards the trigger signal to the ICP-MS unit by starting the laser.

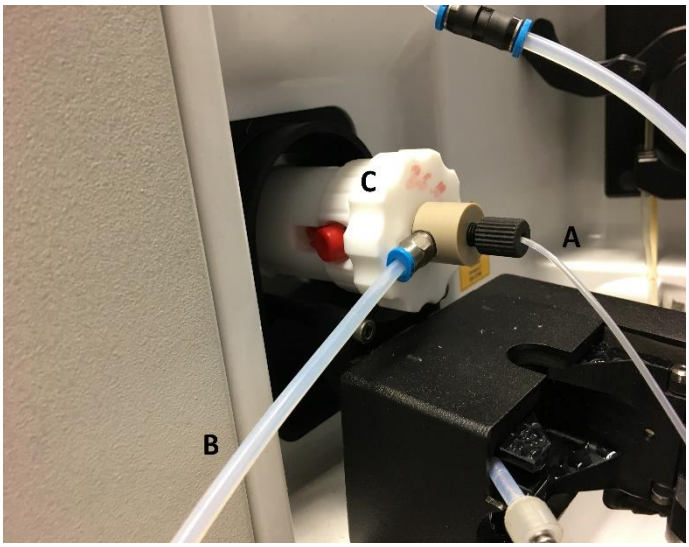

Figure 12: Connection between ICP-MS and LA unit. A: Thinner tube contains helium-aerosol mixture coming from laser ablation system. B: Larger tube contains argon to mix with helium in order to enable the plasma. C: Outside part of plasma torch. Own figure.

The sample to be examined is inserted into the airtight ablation chamber, measured in size and ablated by a UV laser, whereby the sample moves in a µm range under the laser. The diameter of the laser beam can be adapted to the desired resolution.

The resulting aerosol is transported with the carrier gas helium from the ablation chamber to the ICP-MS unit (Fig. 12). There, sample aerosol and helium are mixed with argon to prevent excessive cooling of the plasma torch before it is atomized and ionized in the 9000-10000° C hot argon plasma torch. Transported into the high vacuum of the ICP-MS, the sample particles are then detected time-resolved in terms of their m / z ratio (Fig. 13).

Often the measured values should also be quantified afterwards. For this, it is important to establish an internal measurement standard in order to compensate for fluctuations in the performance of the devices over the duration of the measurement, as well as to create suitable standards for quantification of the data. Here, for example, samples of the same type used can be homogenized and spiked with the elements to be measured, or materials similar to the sample, such as gelatin, can be used [2].

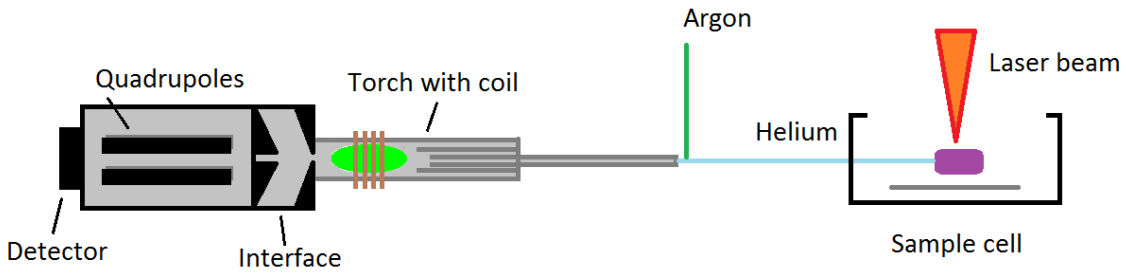

Figure 13: Simplified scheme of whole LA-ICP-MS setup. A UV laser beam passing the cap ablates solid-state sample inside the sample cell. Helium carrier gas transports sample aerosol to argon plasma torch premixed with argon. The plasma atomizes and ionizes the sample aerosol for filtering by quadrupoles and subsequent m/z detection. Own figure.

Multimodal Imaging

Multimodal imaging is a scientific approach in which an attempt is made to generate multiple data sets from different methods in one process or visit. A distinction is made between synchronous and asynchronous approaches, with the latter generating the information in two scans and then aligning them with a program [40, 41]. In this case, processing and correcting the data caused by movements or different positions is a limiting factor. Synchronous approach gives the opportunity to obtain both structural and functional information from just one measurement process, e.g. with use of PET/MRI or PET/CT.

With the combination of different techniques, the investigation of structural and metabolic changes can be combined, both spatially and temporally [42, 43]. Multimodal imaging is therefore a great diagnostic aid as well as a great help in the research regarding the effects of new drugs. PET/MRI is used not only in oncology, but also as a diagnostic tool in cardiology, neurology and psychiatry [44, 45].

The technologies of LA-ICP-MS and PET/MRI could be combined in the future by performing preoperative PET/MRI and postoperative processing, cutting and measuring of removed tissue by means of the method of LA-ICP-MS.

Methods

Protocol for lanthanide labelling of antibodies

For the labelling of lanthanides to the antibodies, Maxpar Antibody Labelling Kits by Fluidigm were used.

As shown in figure 14, the process can be divided into three sub-steps: the first step is the conjugation of the rare earth element to the polymer, the second step is the partial reduction of the disulfide bridges in the heavy chains of the antibodies by use of TCEP (tris(2-carboxyethyl)phosphine), and the final step is to link the element complex to the antibody.

Many of these processes, reactions and incubations occur simultaneously during other steps. The first step is to link the polymer with the lanthanide together. This is followed by a separate washing step for the selected antibody and the polymer-lanthanide complex. The antibody is now partially reduced with TCEP. During a second washing process for the polymer-lanthanide complex, the partially reduced antibody is purified. Finally, the purified antibody is linked to the complex and purified again. The concentration is measured with a spectrophotometer and Antibody Stabilizer PBS is added and stored at 4 ° C until use.

The following antibodies listed in Table 1 have been labeled:

Anti-5-HT1A	Pr 141
Anti-5-HT2A	Pr 141
Anti-5-HT1A	Eu 151
Anti-NMDA/GRIN1	Eu 151

Table 1: List of conjugated antibodies.

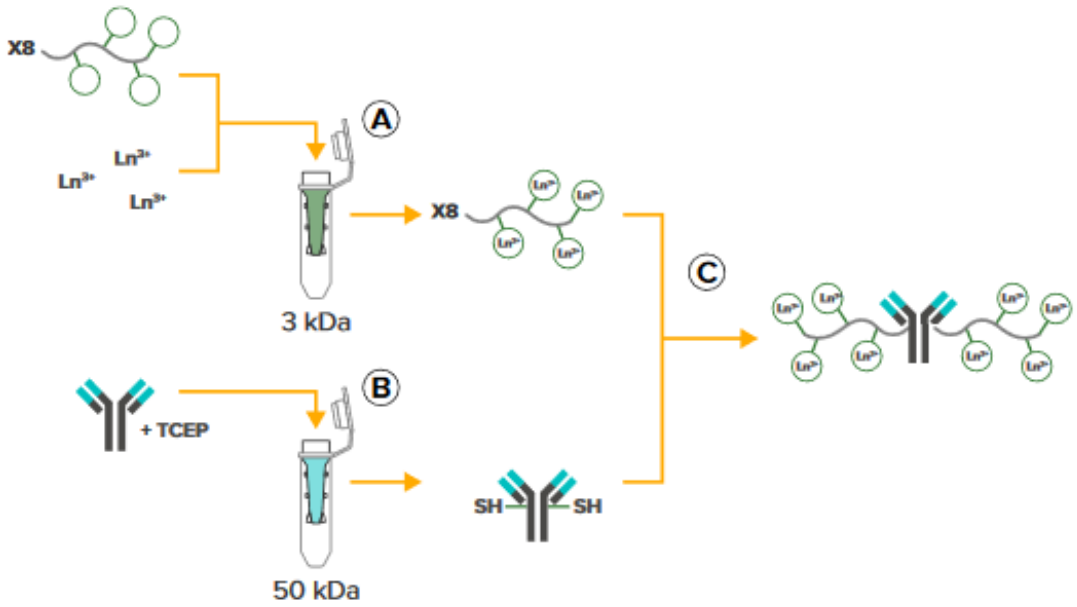

Figure 14: Principle of antigen conjugation with rare earth elements, adapted from Fluidigm [46]. The conjugation takes place in three sub-steps. The polymer is connected to the rare earth element and purified. At the same time, the antibody to be used is washed and partially reduced. Once both steps have been carried out, the lanthanide-polymer complex is linked to the partially reduced antibody and purified again.

Since CyTOF® instruments were not used in this experiment, but LA-ICP-MS methods work stage 40 and 41 of the manufactures labelling protocol have been skipped. Instead, measurements with different concentrations had been performed to assess an optimal working concentration.

LA-ICP-MS measurement

The preparations for performing the measurement of tissue samples by LA-ICP-MS can be divided into the cryosectioning and sample processing as known from IHC. For the frozen sections, indium-tin oxide coated slides are pretreated with a solution to increase the adhesion of the tissue. The rat brain is cut into 10 µm coronal sections on a CyroStar NX-50 and applied to the conductive side of the slide, i.e. the indium-tin oxide coated side. In the following, several immunohistochemical protocols were used and, if necessary, adapted (Appendix II). The main steps here consist of tissue fixation, antigen retrieval if necessary, blocking and antibody incubation.

The sample is then dried and placed in the ablation chamber. Any room air that has been introduced must be removed by flushing sufficiently with helium before the start of the

measurement. In the meantime, the sample is measured with the ablation program and the laser grid is applied. The plasma torch can then be ignited in the ICP-MS and the helium flow of the laser ablation can be turned up to the desired flow rate. This process must be carried out slowly in small steps so as not to extinguish the torch. Since the laser ablation and the ICP-MS measure in a synchronized mode, the ICP-MS does not begin to measure until a trigger signal is issued when the laser is started. As a result, a measured pixel and its measured values can be assigned to each time point of measurement.

Processing of measured images

The counts of the isotopes measured by the ICP-MS instrument control (Fig. 15) and saved by Thermo Scientific Qtegra™ (Fig. 16) are exported as a CSV file. In these CSV files, the measured element counts are assigned to each measurement time. Depending on the size of the section and the number of recorded elements, a file with around a million lines is created.

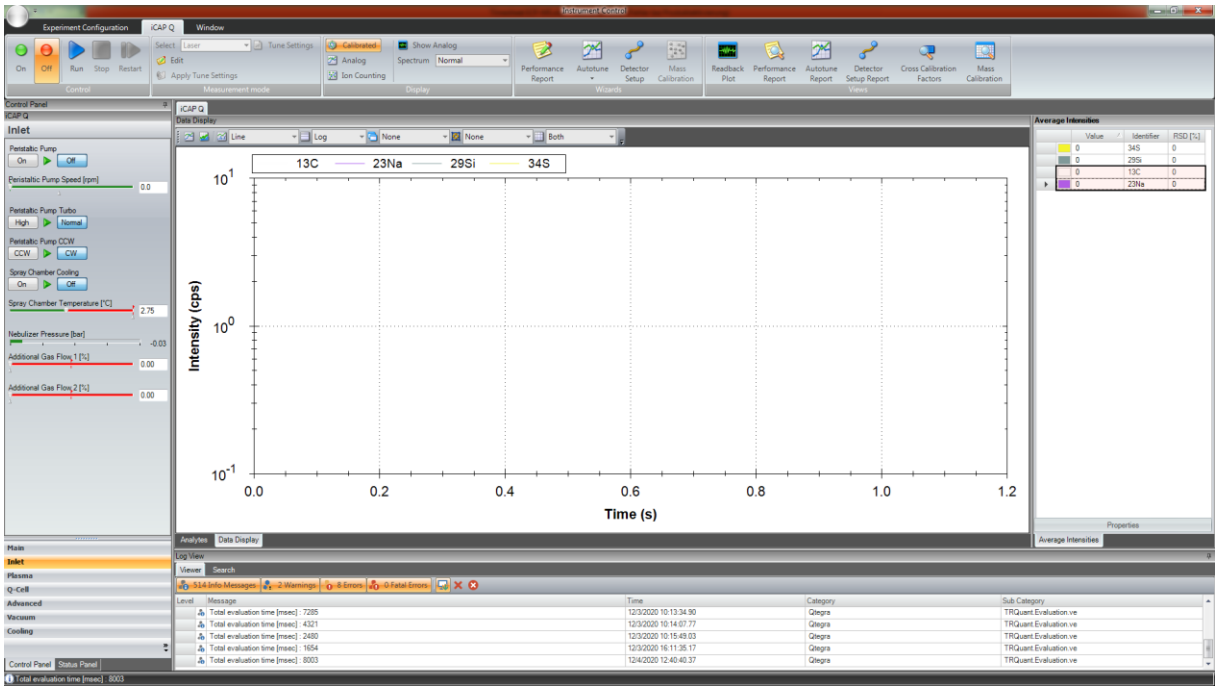

Figure 15: Image of instrument control application for ICP-MS unit. This program ignites the plasma torch, sets the individual isotopes to be measured and monitors the measurement itself. Own figure.

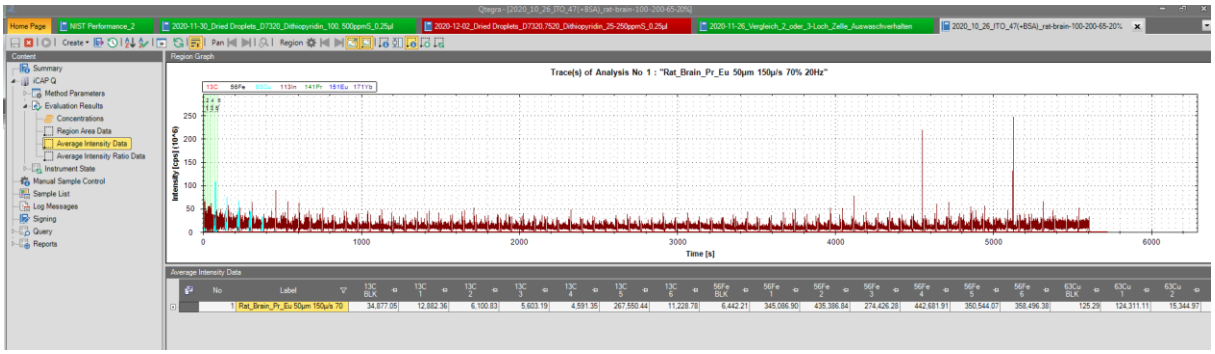

Figure 16: Picture of Qtegra application. With this application the measured counts of the isotopes over time are saved as a CSV data file. Start of the measurement is triggered by initializing the laser beam in a separate laser ablation program. A more detailed picture pf the counts measured is shown and explained below, enlarged, in Figure 19. Own figure.

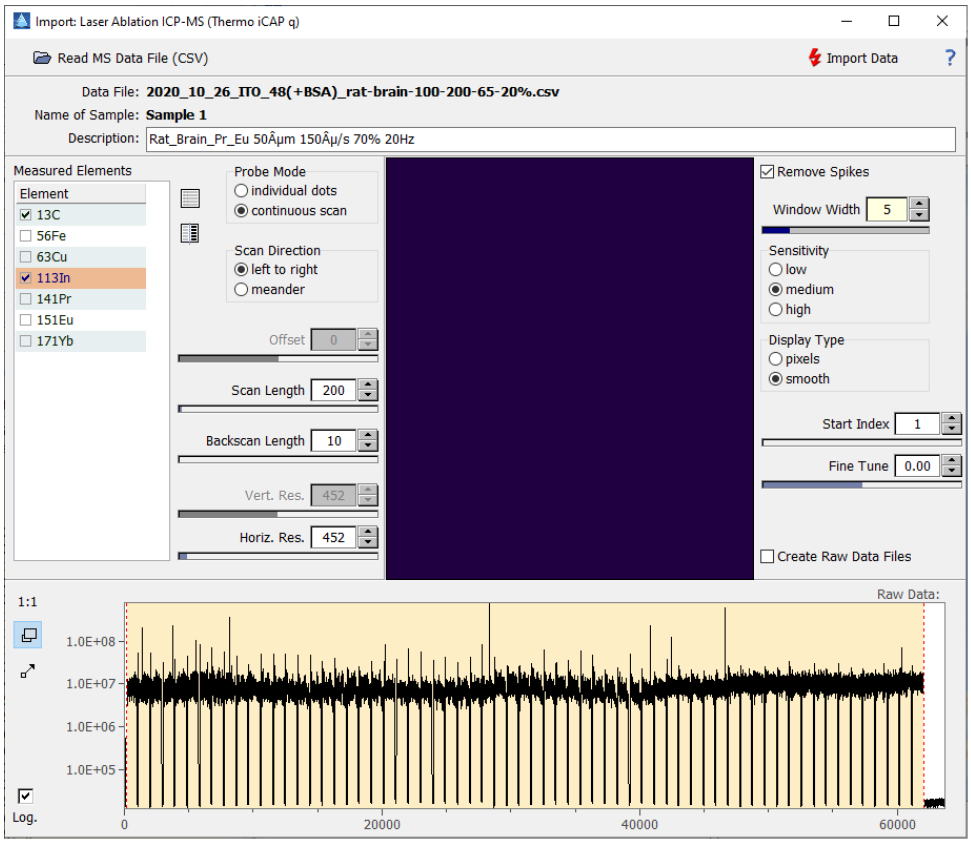

Figure 17: Epina ImageLab program. Adaption of scan and back scan time for data import. Own figure.

The resulting CSV file is now imported into the Epina ImageLab program (Retz, Austria; http://www.imagelab.at/). For this, certain elements of wide distribution are selected and the measured counts are zoomed in. The scan length and back scan can be read from these different measured values (Fig. 17). The scan length is the time that the laser needs to cover a single line

of the grid. The back scan time is the time it takes for the laser to return to the beginning of the following line. Finally, the horizontal resolution is multiplied by the ratio of the x and y axes to compensate for the difference between the measured and the photographed image.

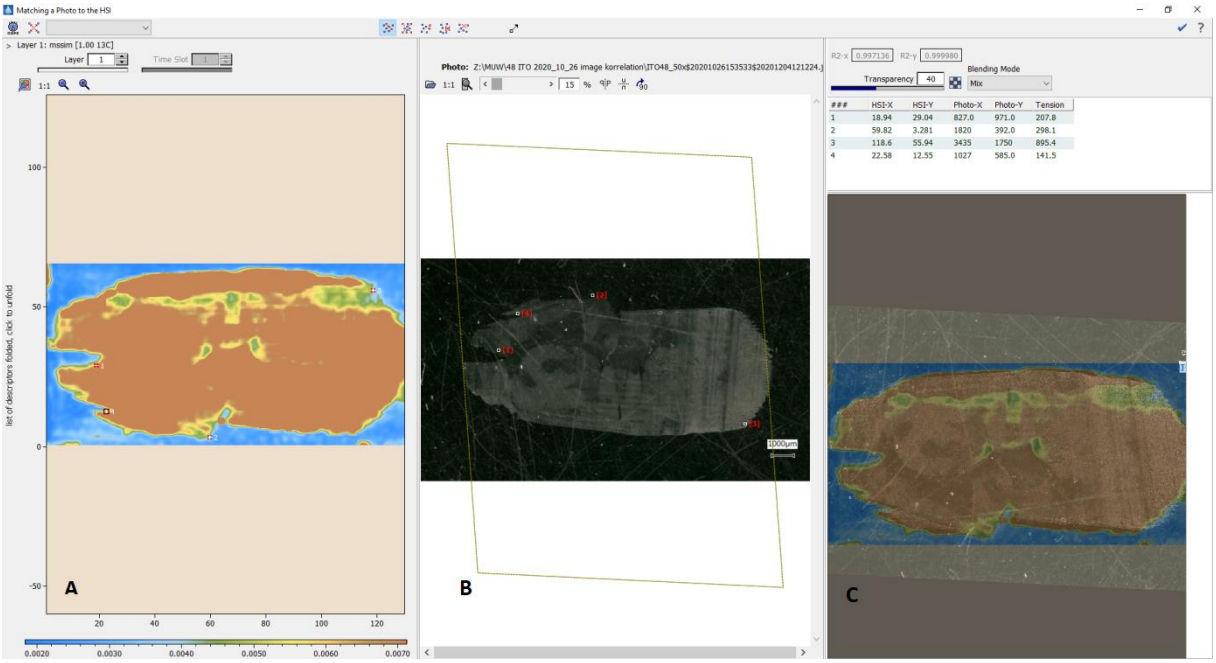

Figure 18: Image of Epina ImageLab. Alignment (C) of measured image (A) and the same slide before processing (B). Own figure.

After the image was imported and loaded, the previously taken photo of the section could be aligned with the measured values (Fig. 18). The left picture shows the distribution of the carbon isotope C13 used for alignment. In this picture, numbered markers are set at prominent points. The more markers are set, the more precise the alignment can be done. The middle image shows the anatomical high-resolution camera image that has to be uploaded for the alignment. In this image, markers are set in the same place as in the image with the carbon distribution. For technical reasons, these images are mirrored horizontally. The image on the right shows the alignment of the image with the measured data.

Unfortunately, it had to be determined that, despite correct alignment of the images, there still could be deviations seen afterwards in the aligned images.

Results

Optimization of laser ablation

For the optimization of the laser ablation, a plan with different parameters was created, with which primarily an optimized laser diameter, feed rate, laser strength and repetition rate should be found.

To be able to narrow down the 84 different parameter combinations as good as possible, single line scans of coronary rat brain slices, incubated with the Anti-5-HT2A antibody labelled with rare earth element praseodymium, were performed (Tab. 2). These single line scans were assessed for ablation visually and by a repeated line scan using mass spectrometry, as you would detect only ^{113} Indium as an internal standard in the second scan.

Feed rate µm/sec	Laser power in %	Repetition Rate in Hz	Spot Size 50 in µm	Spot Size 100 in µm	Spot Size 150 in µm
x2	30	10	50-100-30-10	100-200-30-10	150-300-30-10
		20	50-100-30-20	100-200-30-20	150-300-30-20
	40	10	50-100-40-10	100-200-40-10	150-300-40-10
		20	50-100-40-20	100-200-40-20	150-300-40-20
	50	10	50-100-50-10	100-200-50-10	150-300-50-10
		20	50-100-50-20	100-200-50-20	150-300-50-20
	55	10	50-100-55-10	100-200-55-10	150-300-55-10
		20	50-100-55-20	100-200-55-20	150-300-55-20
	60	10	50-100-60-10	100-200-60-10	150-300-60-10
		20	50-100-60-20	100-200-60-20	150-300-60-20
	65	10	50-100-65-10	100-200-65-10	150-300-65-10
		20	50-100-65-20	100-200-65-20	150-300-65-20
	70	10	50-100-70-10	100-200-70-10	150-300-70-10
		20	50-100-70-20	100-200-70-20	150-300-70-20
x3	30	10	50-150-30-10	100-300-30-10	150-450-30-10
		20	50-150-30-20	100-300-30-20	150-450-30-20
	40	10	50-150-40-10	100-300-40-10	150-450-40-10
		20	50-150-40-20	100-300-40-20	150-450-40-20
	50	10	50-150-50-10	100-300-50-10	150-450-50-10
		20	50-150-50-20	100-300-50-20	150-450-50-20
	55	10	50-150-55-10	100-300-55-10	150-450-55-10
		20	50-150-55-20	100-300-55-20	150-450-55-20
	60	10	50-150-60-10	100-300-60-10	150-450-60-10
		20	50-150-60-20	100-300-60-20	150-450-60-20
	65	10	50-150-65-10	100-300-65-10	150-450-65-10
		20	50-150-65-20	100-300-65-20	150-450-65-20
	70	10	50-150-70-10	100-300-70-10	150-450-70-10
		20	50-150-70-20	100-300-70-20	150-450-70-20

Table 2: Plan for line scan optimization with 84 laser ablation settings. Feed rate describes the speed of the laser movement. Laser feed rate was set two (x2) or three (x3) times the spot size (e.g. if 50 µm laser spot size 100 or 150 µm/sec laser scan speed). Since a measurement would take too long with the same spot size and feed rate (e.g. 50 µm spot size and 50 µm/sec feed rate), this parameter combination was not carried out. Laser power describes the used power of the highest possible laser power in percent (e.g. 65% laser power results in approximately 6 J/cm^2). Repetition rate describes the laser pulse repetition rate with which light is emitted. A laser set with 1 Hz fires 60 times per minute, here the laser fires with 10 or 20 Hz resulting in 10 or 20 laser burst per second. Last three columns describe the used setting, e.g. column spot size 50 µm first row: setting combination50-100-30-10 results in 50 µm laser spot size, 100 µm/sec scan speed, 30% of highest possible laser power and 10 Hz laser repetition rate.

The first scans were performed with a laser diameter of 50 µm and a two and three fold feed rate. In the scans with a laser strength of 30, 40 and 50%, no sufficient removal could be achieved. In case of 150 µm diameter and 300 µm feed rate no sufficient ablation could be detected. Also triple feed rate could be rejected, since even at a repetition rate of 20 Hz the sample was removed very poorly or at high laser power only irregularly. With these first results, focus was put on parameters with a diameter of 50 and 100 and a double feed rate in comparison to the diameter (Tab. 3).

Due to the fact that with a high laser power many parts of the probe outside the laser focus is ablated, scans are performed after drying in a desiccator or at ambient conditions in a laminar flow hood. This additional drying step improved the ablation performance, possibly because residual liquid in the sample is not abruptly vaporized and entrained by the high energy of the laser.

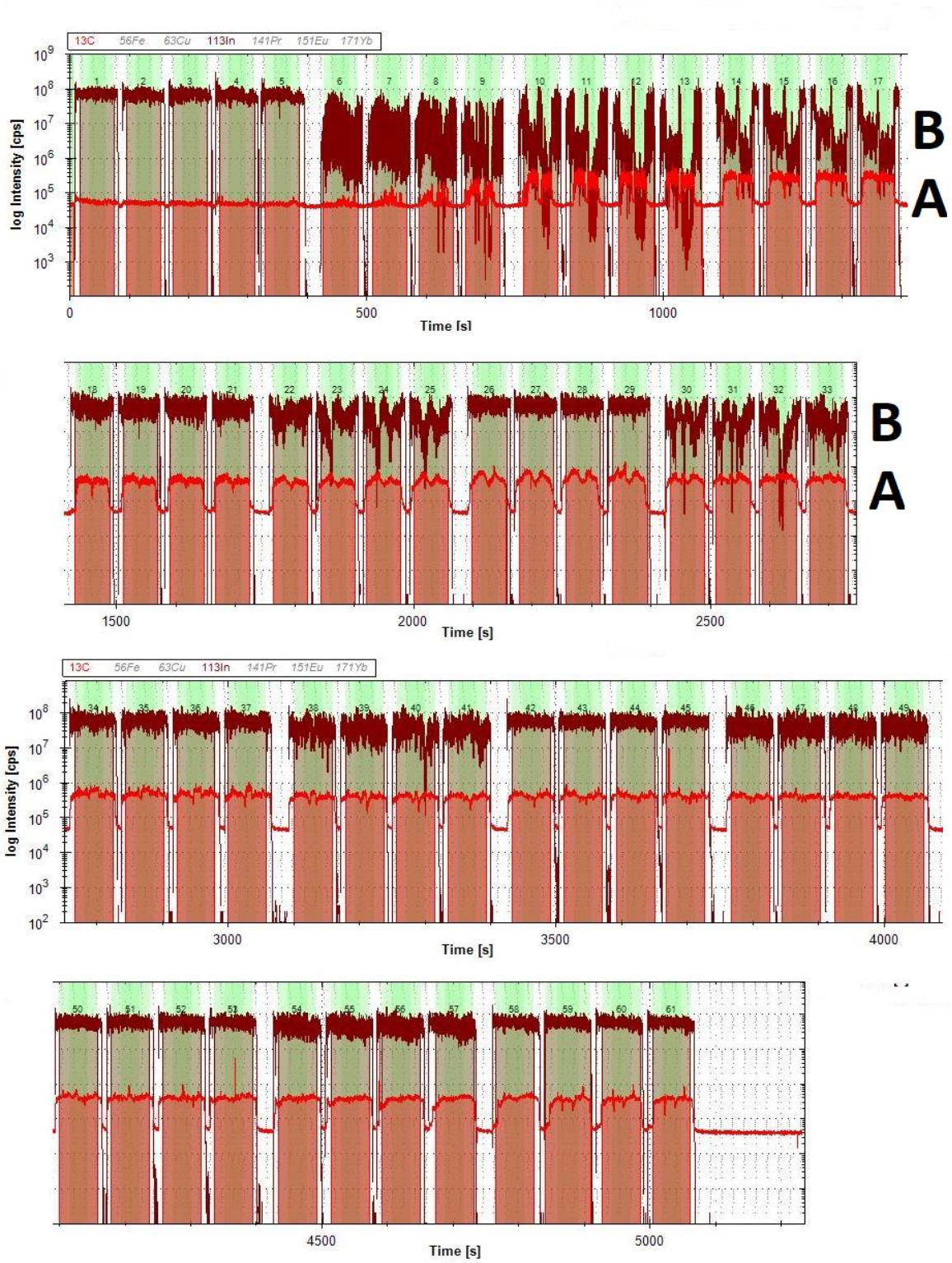

Figure 19: Overview of parameter evaluation measurements. Measurement was made with a laser spot size of 100 µm and a feed rate of 200 µm/sec. In this measurement, the appropriate combination of parameters regarding laser power (in %) and repetition rate (in Hz) should be found with the settings mentioned above. Intensities in logarithmic representation measured in counts per second (cps). The measured ablation of the carbon isotope 13C of a coronary rat brain section is shown in red (A). The erosion of the indium isotope 113In the coating of the measured slide is shown in brown (B). In green the individual measured lines of the slide (scan time; white areas in between are back scan time).

The respective parameter combinations were measured in the following lines:

Line 1-5:	100 µm, 200µm/sec	70%, 20 Hz
Line 6-9:		30%, 10 Hz
Line 10-13:		30%, 20 Hz
Line 14-17:		40%, 10 Hz
Line 18-21:		40%, 20 Hz
Line 22-25:		50%, 10 Hz
Line 26-29:		50%, 20 Hz
Line 30-33:		55%, 10 Hz
Line 34-37:		55%, 20 Hz
Line 38-41:		60%, 10 Hz
Line 42-45:		60%, 20 Hz
Line 46-49:		65%, 10 Hz
Line 50-53:		65%, 20 Hz
Line 54-57:		70%, 10 Hz
Line 58-61:		70%, 20 Hz

Table 3: Parameter combinations for laser setting validation.

In order to find the right strength and repetition rate of the laser for the appropriate laser spot size and feed rate, slides were measured continuously with different parameters (Fig. 19). The first five measured lines (Line 1-5) were only ablation of the ITO slide without tissue section to define the background values of the glass slides, the following rows consist of different parameter combinations of 4 lines each (Tab. 3). The fist and the last combination of parameters correspond to the settings that are usually used in Prof. Limbeck's working group for solid state samples.

It can be seen that in laser settings with a weak laser strength, the ablation of the indium is not sufficiently performed. In the case of medium laser strengths, the indium ablation is only sufficient when combined with a higher repetition rate, 20 Hz. The removal of the tissue sample and the indium as an internal standard was best at 60, 65 and 70%. The most regular ablation of the sample could be observed at 65% and 20 Hz, both with the measured values and with the camera of the laser ablation unit. At 10 Hz, large fluctuations can be observed in all measured lines.

The best results for the ablation of the rat brain sections could ultimately be obtained with the parameters 50µm spot size, 100 µm/sec feed rate and 100 µm spot size, 200 µm/sec feed rate, 20 Hz, 65% laser power. All further scans have been performed with 100 µm laser spot size, 200 µm/sec feed rate, 20 Hz repetition rate and 65% laser power, since with 50µm spot size and 100 µm/sec one measurement including reparations would take up to ten hours.

Optimization of tissue processing

Due to many similar physiological processes in humans and rodents, rats and mice are important model organisms in basic human research [47]. Because of an average length of 2 cm rat brain is easier to handle than a mouse brain. The two brains used in this study were provided by the Institute of Neurology at the Medical University of Vienna. The heads of adult sacrificed rats were cut of with a scissor and the fur was peeled off the skull. The skull was broken open with the help of forceps and pincers and the brain carefully removed. The meninges had been removed and remaining blood was washed off in 1x PBS buffer solution.

A fresh isolated brain was immediately placed in 30% sucrose until the brain had sunk to the ground and then quickly frozen in liquid nitrogen. A second brain was frozen without cryo-protection. In sections of both brains there was a clear reduction in freeze trauma; due to less effort it was continued with the quick freezing process only.

Due to several references in the literature that the fixation of tissue in 4% PFA within several hours is not or only barely sufficient, this step was omitted [48]. Furthermore, prolonged fixation stiffens the tissue and therefore makes it more difficult to cut [49] and might lead to reduced antibody staining [50]. Transcardiac perfusion with 4% PFA was also not an option, as it is a surgical procedure that requires special approval.

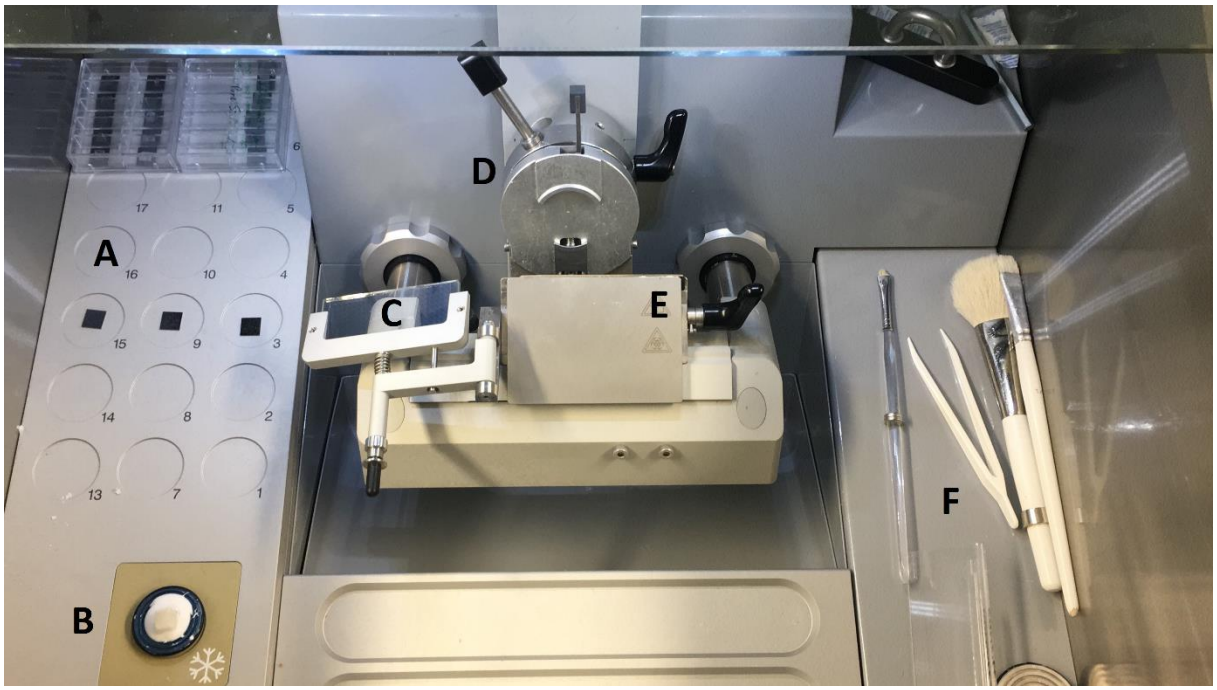

Figure 20: Cooled working chamber of CyroStar NX-50. A: Specimen storage area, B: Cryobar for fast cooling and fixation of specimen, C: Anti-roll glass plate, D: Specimen fixation head, E: Blade slot, F: Storage area for cooled devices for cutting and cleaning (brushes and forceps). Own figure.

The tissue, which was temporarily stored at -80° C degrees until usage, was fixed on a specimen holder with optimal cutting compound (O.C.T.). For this procedure, O.C.T. medium drop of 1 cm diameter was placed in the middle of the specimen holder. The brain tissue was placed with the cerebellum and brain stem upside down facing the specimen holder (Fig. 21). The specimen holder with the brain on it was placed on the cryobar spot for fast cooling an fixation of the tissue to the specimen holder. The brain tissue was then placed in the specimen head cooled to -20° C degrees for 15-20 minutes in order to equilibrate to this temperature.

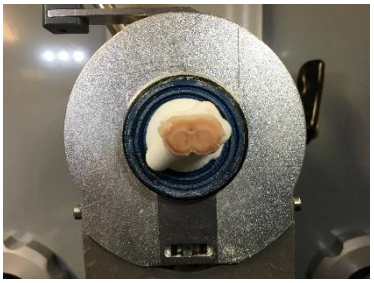

Figure 21: Image of frozen rat brain tissue. Frontal view. The brain is attached to the sample holder (blue) with optimal cutting temperature compound (O.C.T. compound; white).

The sections were applied to the ITO slides by holding the slides stored at room temperature steeply on one of the two long edges of the section. Due to the temperature difference, the sections pulled themselves onto the slide. The ITO slides were pretreated beforehand with an APES acetone solution [51].

After cutting 10 µm cryosections, the slides were immediately fixed in ice-cold acetone for two minutes, dried under ambient conditions and imaged with a high resolution camera (Fig. 22).

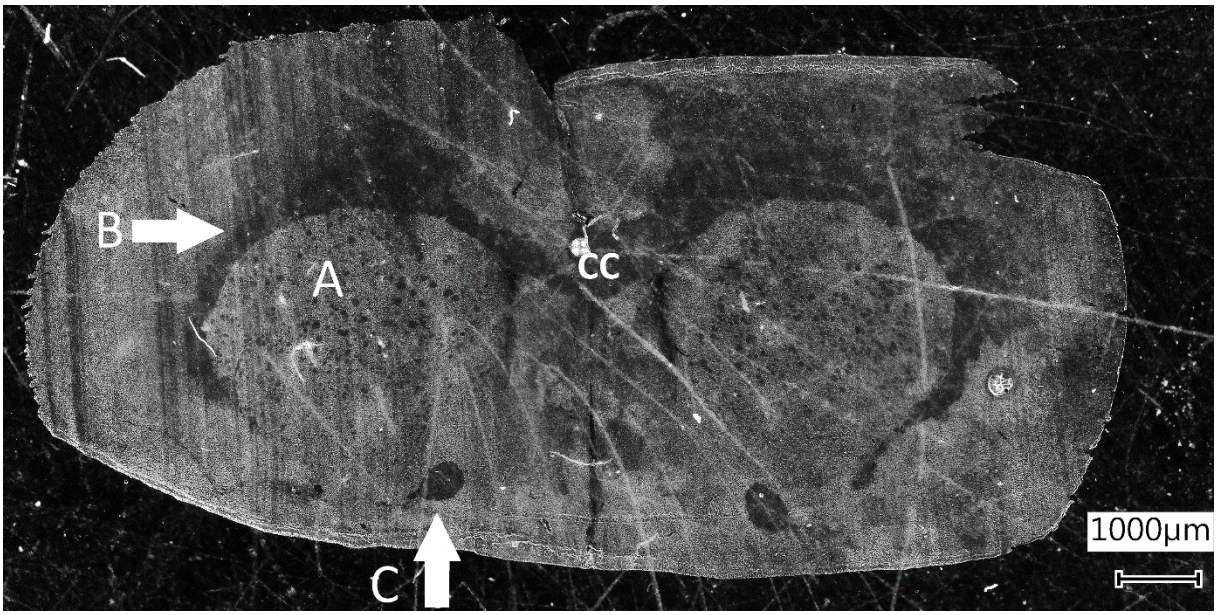

Figure 22: High resolution picture of a coronal rat brain slice. Visible structures: A: caudate-putamen. B: Corpus callosum (CC) and associated subcortical withe matter. C: anterior commissure.

Optimization of antibody incubation

Many different immunohistochemical protocols with different washing steps and incubation procedures had to be tried out and modified in order to find the right setting for these measurements and to avoid high background staining (See Appendix II).

Tests were carried out to fix the sample directly after cutting or before further processing on the day of measurement with acetone or 4% PFA, both pre-chilled to ~4° C.

Different blocking strategies were carried out with BSA and goat serum in 1xTBS or 1xPBS at different concentrations. In addition, washing buffers consisting of 1x TBS or 1xPBS with Triton-X100 concentrations between 0.025 and 0.2% were examined. The use of TBS or PBS turned out to be negligible, especially since alkaline phosphatase detection was not used [52]. The optimal concentration of the detergent in the washing buffer was 0.2%.

In order to find the best-functioning antibody concentration, the concentrations recommended by Fluigigm were measured and each compared twice. It was found that the best result could be achieved at 2.5 µg/ml.

The best results were accomplished repeatedly by fixation pre chilled acetone fixation directly after tissue cutting and placing the slides just before slide processing prior the measurement for 30 minutes from -80 ° C in the -20 ° C refrigerator and finally resting them for 10 minutes at 4° C. This slow thawing process was intended to prevent water condensation on the slide. The sample was then blocked with 300 µl 3% BSA in 1xTBS for one hour. Excess blocking solution was gently shaken off and the slide was incubated with 300 µl antibody mix with 2.5 µg/ml of each antibody. Incubation was performed in a humidity chamber for one hour at room temperature. After incubation, the slide was washed twice with 1xTBS + 0.2% Triton-X for two minutes and again washed twice with 1x TBS for two minutes. Finally, the slide was air dried for 20 to 30 minutes.

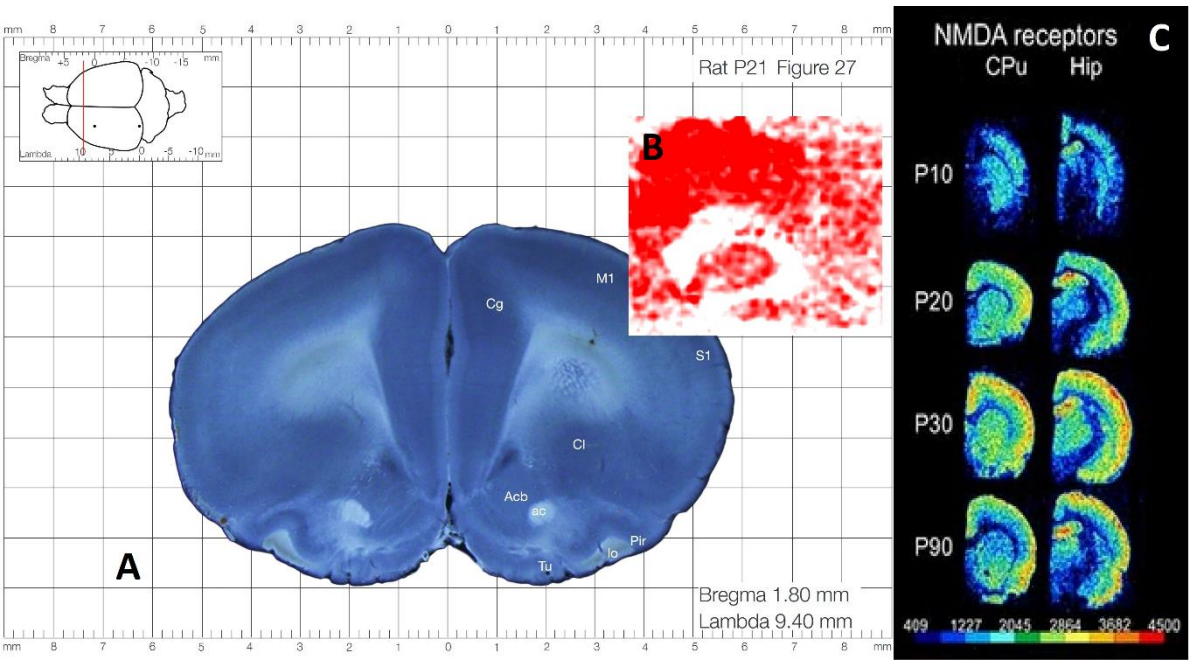

Figure 23: Comparison of coronal anatomical rat brain image, the corresponding coronal NMDA receptor distribution slide measured with LA-ICP-MS and NMDA receptor expression profile. A: Image of a 21 days old brain rat adapted from Khazipov et al.[53]. B: Self-made image of NMDA receptor distribution measured with LA-ICP-MS. C: NMDA receptor distribution profile showing several coronal slices, adapted from Behuet et al. [54].

First exploratory measurements with an antibody specific for NMDA bound to a polymer with europium have shown that this method in comparison with the literature is suitable for successfully measuring of biological targets (Fig. 23). The section measured with LA-ICP-MS was cut in approximately the same area as the sections of the anatomical atlas by Roustem

Khazipov et al. from 2015 [53]. In comparison, an autoradiographic image of the NMDA receptor distribution detected with 3H-MK-801 by Sabrina Behuet et al. published in 2019 [54]. In both images made with LA-ICP-MS and with autoradiography it can be clearly seen that the NMDA receptors in the area of the corpus callosum between the cortex and caudate-putamen are not detected, as they are not supposed to be expressed in these regions. No area specific quantification in different cortical areas have been done.

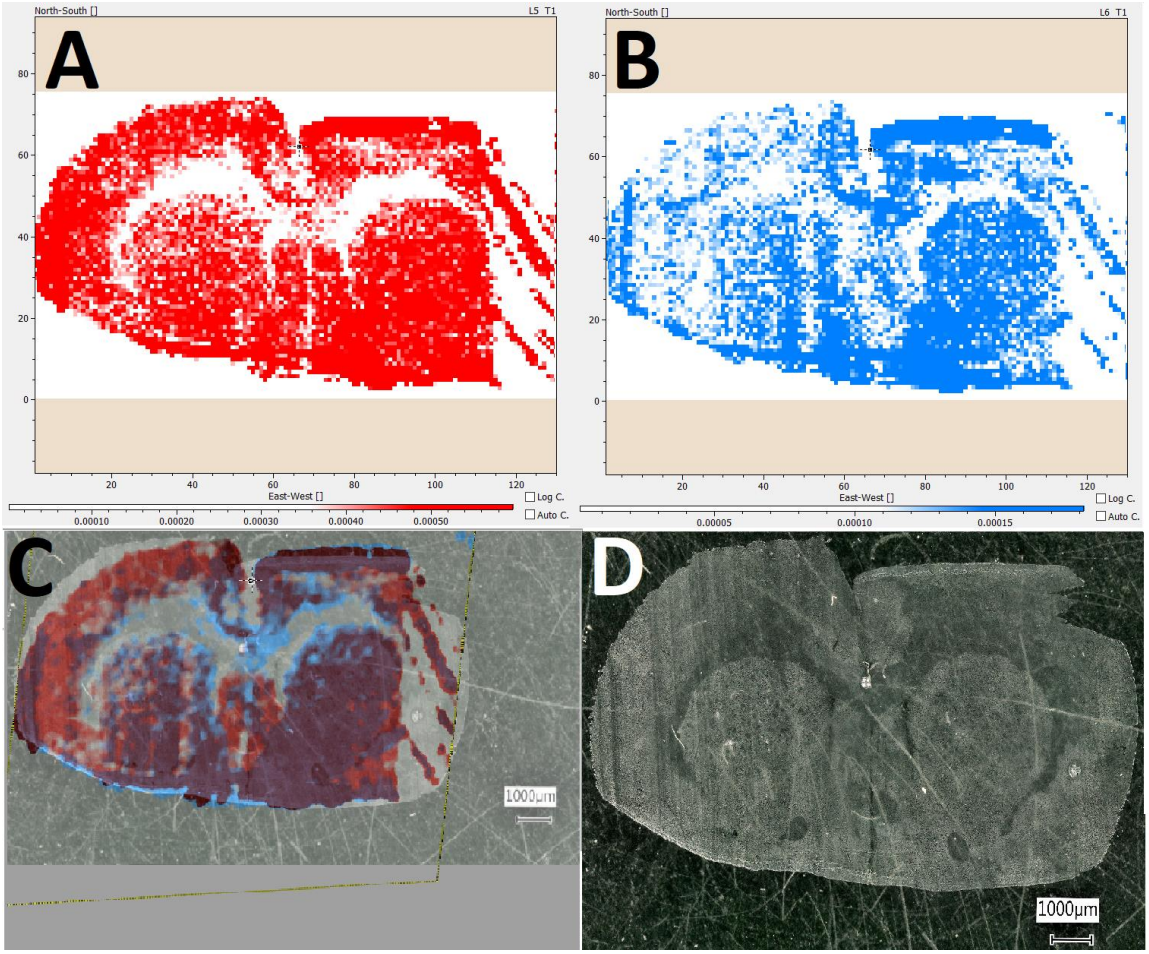

Figure 24: Measurement of coronar rat brain slice on ITO slide. A: Distribution of 141Pr-5HT2A antibody. B: Distribution of 151Eu-5HT1A antibody. C: Measured images aligned with the high-resolution image rat brain slice before processing and incubation for LA-ICP-MS. D: high-resolution image rat brain slice before processing and incubation for LA-ICP-MS. Scratch on tissue on left side due to edges on glass anti-roll plate. Tissue smear on right side caused by accident during processing. Own figure.

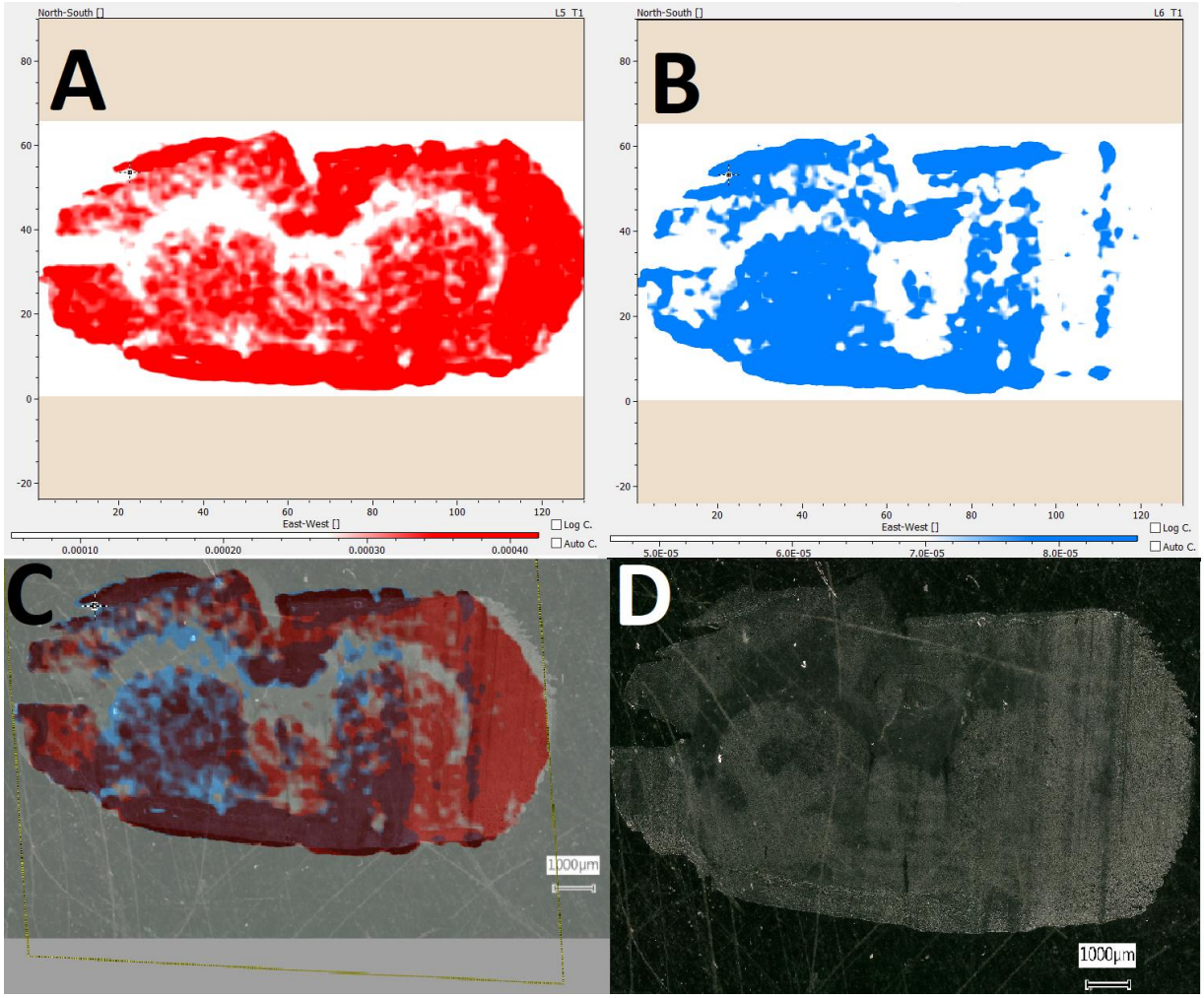

Figure 25: Measurement of coronar rat brain slice on ITO slide, slightly more posterior than the previous slide. A: Distribution of 141Pr-5HT2A antibody. B: Distribution of 151Eu-5HT1A antibody. C: Measured images aligned with the high-resolution image rat brain slice before processing and incubation for LA-ICP-MS. D: high-resolution image rat brain slice before processing and incubation for LA-ICP-MS. Scratch on tissue on left side due to edges on glass anti-roll plate. Tissue smear on right side caused by accident during processing. Own figure.

Further measurements with two simultaneously measured serotonin receptors 5HT1A and 5HT2A also suggest that the simultaneous measurement of several carriers is also possible. Unfortunately, the graphical representation of several simultaneous measured carriers is not possible with the used program Epina ImageLab (Retz, Austria; http://www.imagelab.at/), because the individual colors cannot be represented in a graduated manner.

Quantification with gelatin standards

The steps of the establishment of gelatin standards for target quantification were done together with bachelor student Nina Plischek.

For the quantification of the targets measured, gelatin standards with used elements have been made [55, 56].

1 gram of gelatine has been dissolved in 8.98 ml dH_2O at 55° C.

A stock solution of 1000ppb with the elements praseodymium, europium and ybbterium in 1% HNO_3 was prepared (Tab. 4).

Element	Measured conc.	Initial weight
Pr 141	989 µg/g	0.0851 g
Eu 151	992µg/g	0.0859 g
Yb 171	980µg/g	0.0860 g

Table 4: Stock mixture for quantification with gelatin standards.

With this 1000 ppb stock solution, further tubes with 200 ppb, 50 ppb, 10 ppb and a blank were made (Tab. 5).

Conc	Initial weight	HNO_3 1%
200 ppb	0.0289 g	0.0685 g
50 ppb	0.0751 g	0.9123 g
10 ppb	0.0148 g	0.9809 g

Table 5: Diluted concentrations in 200, 50 and 10 ppb, diluted with 1% HNO3.

The dissolved gelatin was aliquoted into a total of five 50 ml Falcon tubes of two ml each and the respective stock solutions were added as follows. Yttrium was added to all tubes as an internal standard (Tab. 6).

Tube	Conc.	Weight Yttrium	Weight stock sol.
1	Blank	0.0083 g	0.0182 g 1% HNO_3
2	10 ppb	0.0085 g	0.0196 g of 10 ppb st. sol.
3	50 ppb	0.0085 g	0.0196 g of 50 ppb st. sol.
4	200 ppb	0.0090 g	0.0203 g of 200 ppb st. sol.
5	1000 ppb	0.0098 g	0.0190 g of 1000 ppb st. sol.

Table 6: Gelatine quantification standards with added Yttrium in order to obtain an internal standard.

The spiked gelatin was homogenized with a vortex and degassed for one hour at 55 ° C in an ultrasonic water bath in order to get the gelatin free of air bubbles.

The degassed gelatin was now further prepared for the measurement on the ITO slides. Two different methods were compared: on the one hand the measurement of individual drops and on the other hand the measurement of gelatin slices.

20 µl of each of the five concentrations were applied to a cold or a preheated ITO slide. The slides were dried in a convection oven at 115 ° C for one hour. After the slide had cooled down, all slides were stored at -80 ° C until the measurement started.

The remaining gelatin was poured into 3.5 cm Petri dishes and put in the refrigerator at 4 ° C overnight to gel. Small cubes were then cut out of the gelatin, attached to the sample holder with OCT medium and cut with the cryotom to 10 µm sections at -20 ° C. This process was carried out for all 5 concentrations.

The quantitation standards were measured with the same parameters in line scan mode as the brain samples. Because of the strong optical unevenness on the surface of the dried single droplets, only gelatin sections were further measured. Nevertheless, both variants showed the correct concentrations in a comparison of the calculated standard curve (Fig. 26). The value for 1000 ppb has been removed from the graph as it seems to be an outlier. In the case of gelatin standards with such high concentrations, namely four times 1000 ppb element standard, there can be a large non-representative variance.

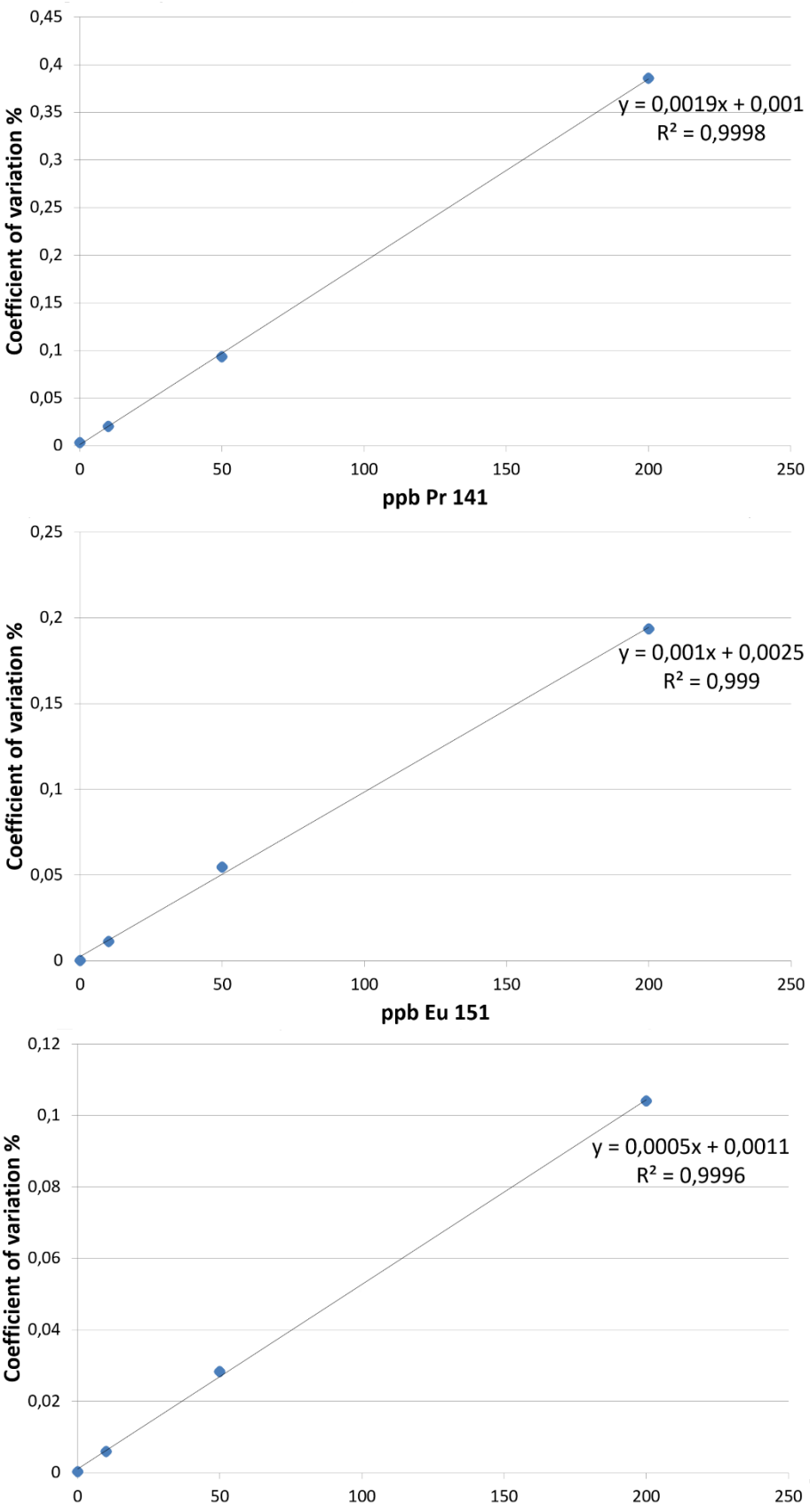

Figure 26: Simple linear regression for the measured elements presodymium, europium and ybbterium in 10 ppb, 50 ppb and 200 ppb. At the end of the calibration line, the associated linear equation and the coefficient of determination can be found. All three coefficients of determination provide an almost perfect linear relationship of over 99.9%.

By integrating the measured gelatin standards spiked with rare earth elements, the measured counts could be quantified. The two data sets of the gelatin standards and the measured rat brain sections were normalized to the isotope 13C. The resulting data are ppb (parts per billion) or µg/kg.

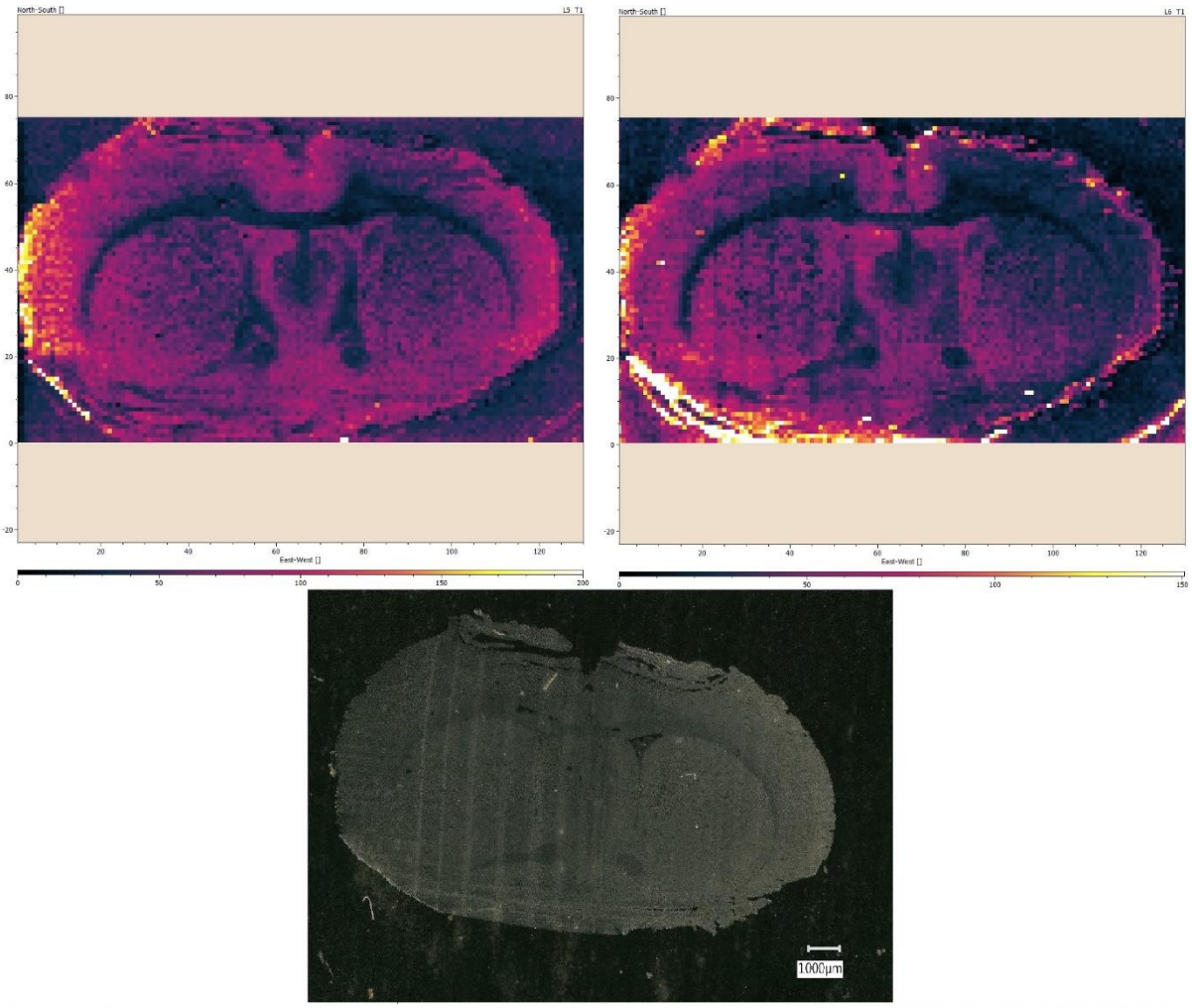

Figure 27: Quantified measurement of coronar rat brain slice on ITO slide, in contrast to Figure 24 and 25 where data from gelatine standards for quantification had not been included. Upper left: Distribution of 141Pr-5HT2A antibody. Upper right: Distribution of 151Eu-5HT1A antibody. Lower: High resolution image of measured coronar rat brain slice after cutting and fixation.

Discussion

In this thesis, initial experiences with LA-ICP-MS could be gained and the work steps for rodent brain tissue could be optimized. With the optimization of the link between IHC and LA-ICP-MS, it can be shown that this method is an important tool for a faster and easier understanding of the protein distributions in biological samples. Since repeated washing and incubation steps can be avoided, unlike with conventional IHC, a significant time saving method can be found here while measuring several targets at the same time.

The comparison of this work with the results in the published literature suggests that parts of the results of this work are consistent with the previous state of knowledge. In the following image (Fig. 28), the distribution of the serotonin receptor 5-HT_{2A} measured by LA-ICP-MS is compared with the results of Weber & Andrade, 2010 [57]. It can be seen that the antibodies bind in both cases in the cortical areas and the basal ganglia, but not in the corpus callosum.

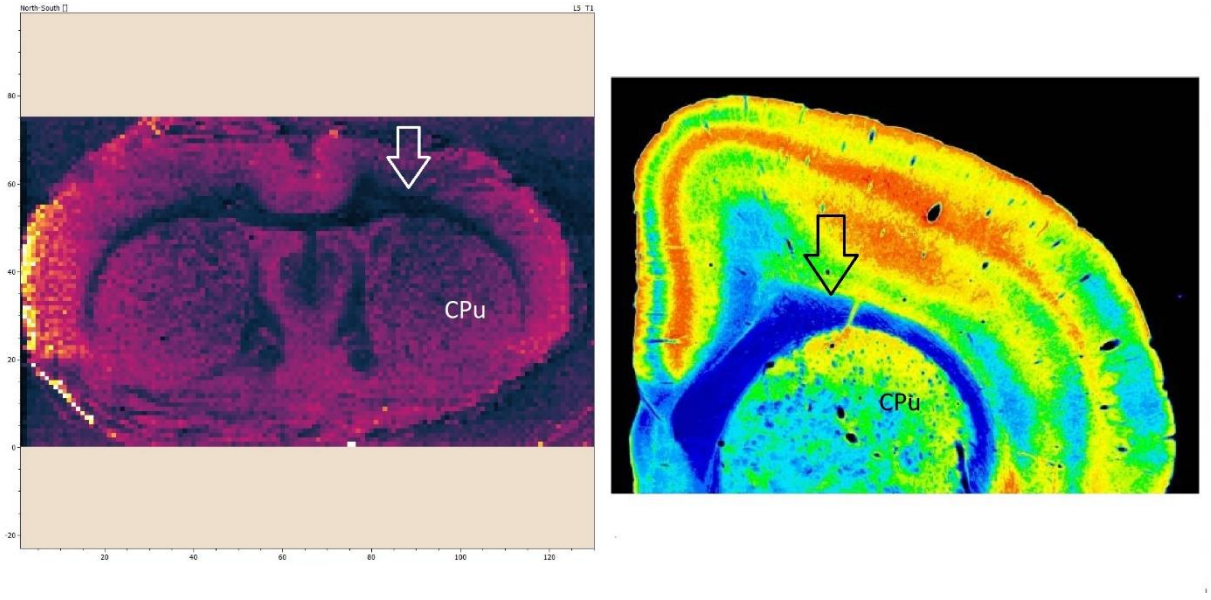

Figure 28: Comparision of target measured with LA-ICP-MS and IHC. Left image: Distribution of 141Pr-5HT_{2A} antibody. Right: Image of pseudocolorised IHC of 5-HT_{2A} adapted from [57]. In both images antibody can be found in cortical areas and caudate-putamen (CPu), but not in corpus callosum (arrows).

In the case of the serotonin receptor 5-HT_{1A} (Fig.29), further tests should be carried out with other antibodies. Contrary to expectations, the antibody binds in areas of the caudate-putamen,

although it has been observed differently in the literature [58, 59]. These results must be viewed very critically and repeated with antibodies of other manufacturer.

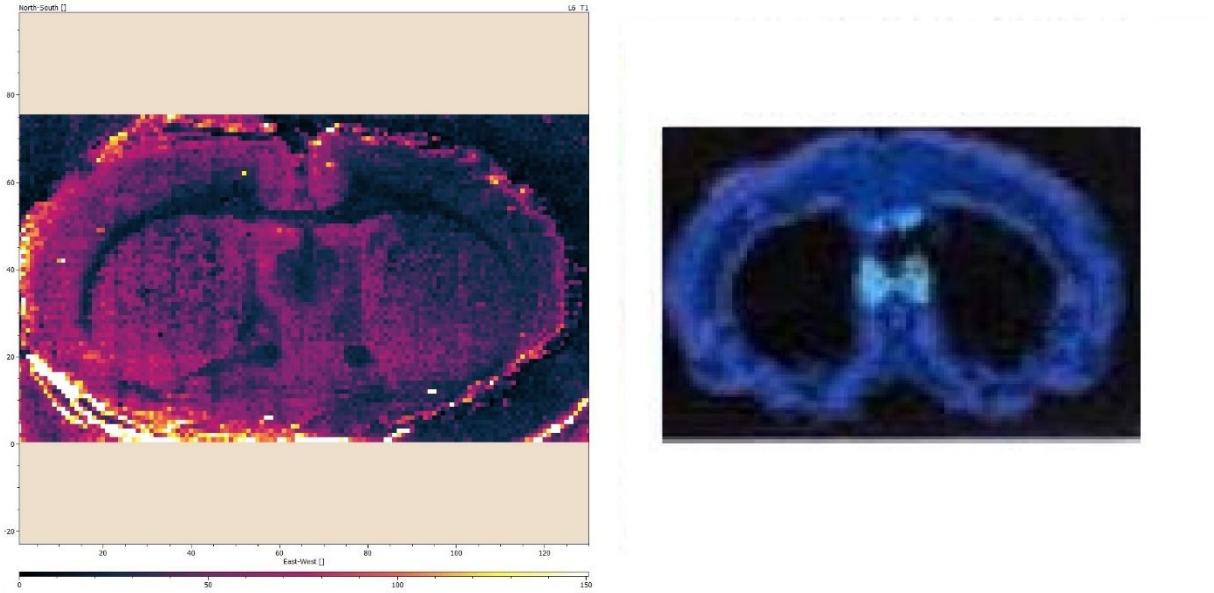

Figure 29: Comparision of target measured with LA-ICP-MS and IHC. Left image: Distribution of 151Pr-5HT$_{1A}$ antibody. Right image: Adapted autoradiographic image of 5-HT$_{1A}$ receptor distribution with receptor agonist 8-OH-DPAT labelled with tritium [58].

The disadvantage, however, is a lower spatial resolution compared to common immunohistochemistry [60] and the time it takes to measure an entire rat brain or, for example, a human hippocampus. In theory, you can cut a rat brain two centimeters long in up to 2000 sections of 10 µm each. With a measurement time of 1.5 to 2 hours per cut, this results in up to 4000 hours of pure measurement time without around 4 hours of preparations per measurement day. This problem can be counteracted by measuring only every 50 or 100 µm in the LA-ICP-MS. For measurements of every 100 µm, a period of at least 3 months with 5 days of measurement per week must be expected. Still, further attempts to improve the presentation of cortical and subcortical structures with even smaller laser settings around 50 µm laser spot diameter are needed.

Another limitation is the often discussed reproducibility of studies with antibodies, not only between different working groups, but also between two lab technician. Many scientists claim a batch-to-batch variability; the Swedish consortium around Human Protein Atlas even found that of 20,000 investigated antibodies against proteins in the human genome, only 50% can be used effectively to track the protein distribution in the human body [61]. There is an open and long-standing discussion about who is responsible for the validation of the antibodies.

Unfortunately, there were problems with kits that clearly advertised the detection of certain proteins, but then recognized completely different targets [62]. In this case the responsibility seems to lie clearly with the producer. On the other hand, with individual antibodies it is understandable that the validation of these lie in the responsibility of the scientist [63].

If you consider that the rare earth elements consist of 14 stable elements and these consist of 44 stable isotopes, the advantage of this method clearly outweighs. The company Fluidigm offers 12 lanthanides with a total of 35 different isotopes in its range, but isobaric interference and reaction with atomic oxygen must be considered when selecting the isotopes in order to get representative images. Due to the range of isotopes, more targets can be detected per measurement run than with immunohistochemical approach. Furthermore, it is a important advantage that these elements hardly occur in biological samples and so the measured signal to noise ratio is significantly better than with conventional IHC.

There are hardly any limits to the desired targets of the antibodies, since not only membrane-associated targets can be measured, as in this work. With help of stronger detergents, cell membranes can be easily permeabilized and thus intracellular targets can be marked too.

As an outlook, LA-ICP-MS gives an important technique to correlate data obtained from multimodal proteomics by laser ablation ICP-MS in, for example, surgically removed hippocampi from patients suffering from temporal lobe epilepsy, with data from spatial transcriptomic. Here, data obtained with PET could be compared in order to verify PET as the gold standard in diagnostics and clinical research. Due to the high spatial resolution of modern systems in the µm range, receptor and neurotransmitter distributions can be displayed very precisely. As an second prospect, these two-dimensional images from mass spectrometry imaging could be aligned in order to create three-dimensional atlases for protein distributions [64], in genetic models as well as in extracted tissue of patients suffering from various neurological or psychiatric diseases.

References

[1] P. Sylvester and S. Jackson, "A Brief History of Laser Ablation Inductively Coupled Plasma Mass Spectrometry (LA–ICP–MS)," *Elements*, vol. 12, pp. 307–310, Oct. 2016, doi: 10.2113/gselements.12.5.307.

[2] A. Limbeck, P. Galler, M. Bonta, G. Bauer, W. Nischkauer, and F. Vanhaecke, "Recent advances in quantitative LA-ICP-MS analysis: challenges and solutions in the life sciences and environmental chemistry," *Anal. Bioanal. Chem.*, vol. 407, no. 22, pp. 6593–6617, Sep. 2015, doi: 10.1007/s00216-015-8858-0.

[3] J. Lin, Y. Liu, Y. Yang, and Z. Hu, "Calibration and correction of LA-ICP-MS and LA-MC-ICP-MS analyses for element contents and isotopic ratios," *Solid Earth Sci.*, vol. 1, no. 1, pp. 5–27, 2016, doi: https://doi.org/10.1016/j.sesci.2016.04.002.

[4] J. Bianga *et al.*, "Complementarity of MALDI and LA ICP mass spectrometry for platinum anticancer imaging in human tumor," *Metallomics*, vol. 6, Jul. 2014, doi: 10.1039/c4mt00131a.

[5] A. Balbekova *et al.*, "Fourier Transform Infrared (FT-IR) and Laser Ablation Inductively Coupled Plasma-Mass Spectrometry (LA-ICP-MS) Imaging of Cerebral Ischemia: Combined Analysis of Rat Brain Thin Cuts Toward Improved Tissue Classification.," *Appl. Spectrosc.*, vol. 72, no. 2, pp. 241–250, Feb. 2018, doi: 10.1177/0003702817734618.

[6] M. Bonta, S. Török, B. Hegedus, B. Döme, and A. Limbeck, "A comparison of sample preparation strategies for biological tissues and subsequent trace element analysis using LA-ICP-MS," *Anal. Bioanal. Chem.*, vol. 409, no. 7, pp. 1805–1814, 2017, doi: 10.1007/s00216-016-0124-6.

[7] C. Kraus, E. Castrén, S. Kasper, and R. Lanzenberger, "Serotonin and neuroplasticity - Links between molecular, functional and structural pathophysiology in depression.," *Neurosci. Biobehav. Rev.*, vol. 77, pp. 317–326, Jun. 2017, doi: 10.1016/j.neubiorev.2017.03.007.

[8] D. J. Nutt, "Relationship of neurotransmitters to the symptoms of major depressive disorder.," *J. Clin. Psychiatry*, vol. 69 Suppl E, pp. 4–7, 2008.

[9] S. Magaki, S. A. Hojat, B. Wei, A. So, and W. H. Yong, "An Introduction to the Performance of Immunohistochemistry.," *Methods Mol. Biol.*, vol. 1897, pp. 289–298, 2019, doi: 10.1007/978-1-4939-8935-5_25.

[10] A. M. Feyissa and W. O. Tatum, "Adult EEG.," *Handb. Clin. Neurol.*, vol. 160, pp. 103–124, 2019, doi: 10.1016/B978-0-444-64032-1.00007-2.

[11] B. P. Keogh and J. W. Henson, "Clinical manifestations and diagnostic imaging of brain tumors.," *Hematol. Oncol. Clin. North Am.*, vol. 26, no. 4, pp. 733–755, Aug. 2012, doi: 10.1016/j.hoc.2012.05.002.

[12] H. Herzog and C. Lerche, “Advances in Clinical PET/MRI Instrumentation.,” *PET Clin.*, vol. 11, no. 2, pp. 95–103, Apr. 2016, doi: 10.1016/j.cpet.2015.09.001.

[13] S. J. Dienel and D. A. Lewis, “Alterations in cortical interneurons and cognitive function in schizophrenia.,” *Neurobiol. Dis.*, vol. 131, p. 104208, Nov. 2019, doi: 10.1016/j.nbd.2018.06.020.

[14] B. Kerner, “Glutamate Neurotransmission in Psychotic Disorders and Substance Abuse.,” *Open Psychiatr. J.*, vol. 3, pp. 1–8, Jan. 2009, doi: 10.2174/1874354400903010001.

[15] J. Dean and M. Keshavan, “The neurobiology of depression: An integrated view.,” *Asian J. Psychiatr.*, vol. 27, pp. 101–111, Jun. 2017, doi: 10.1016/j.ajp.2017.01.025.

[16] M. Woelfer, V. Kasties, S. Kahlfuss, and M. Walter, “The Role of Depressive Subtypes within the Neuroinflammation Hypothesis of Major Depressive Disorder.,” *Neuroscience*, vol. 403, pp. 93–110, Apr. 2019, doi: 10.1016/j.neuroscience.2018.03.034.

[17] A. Adell, P. Celada, M. T. Abellán, and F. Artigas, “Origin and functional role of the extracellular serotonin in the midbrain raphe nuclei.,” *Brain Res. Brain Res. Rev.*, vol. 39, no. 2–3, pp. 154–180, Sep. 2002, doi: 10.1016/s0165-0173(02)00182-0.

[18] J.-P. Hornung, “The human raphe nuclei and the serotonergic system.,” *J. Chem. Neuroanat.*, vol. 26, no. 4, pp. 331–343, Dec. 2003, doi: 10.1016/j.jchemneu.2003.10.002.

[19] R. J. Brezski and G. Georgiou, “Immunoglobulin isotype knowledge and application to Fc engineering.,” *Curr. Opin. Immunol.*, vol. 40, pp. 62–69, Jun. 2016, doi: 10.1016/j.coi.2016.03.002.

[20] D. N. Forthal, “Functions of Antibodies,” *Microbiol. Spectr.*, vol. 2, no. 4, pp. 1–17, Aug. 2014, [Online]. Available: https://pubmed.ncbi.nlm.nih.gov/25215264.

[21] H. A. Parray *et al.*, “Hybridoma technology a versatile method for isolation of monoclonal antibodies, its applicability across species, limitations, advancement and future perspectives,” *Int. Immunopharmacol.*, vol. 85, p. 106639, Aug. 2020, doi: 10.1016/j.intimp.2020.106639.

[22] BIO RAD, “Antibodies Conjugated to Fluorophores.” https://www.bio-rad-antibodies.com/fluorophores.html.

[23] abcam, “Conjugated antibodies for immunofluorescence and flow cytometry.” https://www.abcam.com/primary-antibodies/highly-validated-antibody-conjugates.

[24] Thermo Fisher Scientific, “Bond-Breaker™ TCEP Solution, Neutral pH.” https://www.thermofisher.com/order/catalog/product/77720#/77720.

[25] J. A. Burns, J. C. Butler, J. Moran, and G. M. Whitesides, “Selective reduction of disulfides by tris(2-carboxyethyl)phosphine,” *J. Org. Chem.*, vol. 56, no. 8, pp. 2648–2650, Apr. 1991, doi: 10.1021/jo00008a014.

[26] D. C. Bundy, “Autoradiography,” *Curr. Protoc. Protein Sci.*, vol. 10, no. 1, pp. 10.11.1-10.11.6, Dec. 1997, doi: https://doi.org/10.1002/0471140864.ps1011s10.

[27] I. Manuel *et al.*, "Neurotransmitter receptor localization: from autoradiography to imaging mass spectrometry.," *ACS Chem. Neurosci.*, vol. 6, no. 3, pp. 362–373, Mar. 2015, doi: 10.1021/cn500281t.

[28] E. S. Lasers, "NWR 213 Laser Ablation System." http://www.nwrlasers.com/laserablation/nwr213/.

[29] C. M. Pacella, L. Breschi, D. Bottacci, and L. Masotti, "Physical Principles of Laser Ablation," in *Image-guided Laser Ablation*, C. M. Pacella, T. Jiang, and G. Mauri, Eds. Cham: Springer International Publishing, 2020, pp. 7–18.

[30] V. Knappe, F. Frank, and E. Rohde, "Principles of lasers and biophotonic effects.," *Photomed. Laser Surg.*, vol. 22, no. 5, pp. 411–417, Oct. 2004, doi: 10.1089/pho.2004.22.411.

[31] J. Evers, P. Klüfers, R. Staudigl, and P. Stallhofer, "Czochralski's Creative Mistake: A Milestone on the Way to the Gigabit Era," *Angew. Chemie Int. Ed.*, vol. 42, no. 46, pp. 5684–5698, Dec. 2003, doi: https://doi.org/10.1002/anie.200300587.

[32] M. Eichenseer, "Aufbau und Charakterisierung eines hochstabilen Nd.YAG Lasers für ein Indium Frequenznormal," Ludwig-Maximilians-Universität München, 2003.

[33] J. Lingott, "Untersuchungen zur Aufnahme und Verteilung von gadoliniumbasierten Kontrastmitteln in biologischen Proben mittels Laserablation mit induktiv gekoppelter Plasma-Massenspektrometrie," Humboldt-Universität zu Berlin, Mathematisch-Naturwissenschaftliche Fakultät, 2016.

[34] R. S. Houk, V. A. Fassel, G. D. Flesch, H. J. Svec, A. L. Gray, and C. E. Taylor, "Inductively coupled argon plasma as an ion source for mass spectrometric determination of trace elements," *Anal. Chem.*, vol. 52, no. 14, pp. 2283–2289, Dec. 1980, doi: 10.1021/ac50064a012.

[35] Robert Thomas, *Practical Guide to ICP-MS*. New York, Basel: Marcel Dekker, Inc., 2004.

[36] T. Ubide, C. A. McKenna, D. M. Chew, and B. S. Kamber, "High-resolution LA-ICP-MS trace element mapping of igneous minerals: In search of magma histories," *Chem. Geol.*, vol. 409, pp. 157–168, 2015, doi: https://doi.org/10.1016/j.chemgeo.2015.05.020.

[37] J. S. Becker and J. S. Becker, "Imaging of metals, metalloids, and non-metals by laser ablation inductively coupled plasma mass spectrometry (LA-ICP-MS) in biological tissues.," *Methods Mol. Biol.*, vol. 656, pp. 51–82, 2010, doi: 10.1007/978-1-60761-746-4_3.

[38] D. J. Hare *et al.*, "Imaging Metals in Brain Tissue by Laser Ablation - Inductively Coupled Plasma - Mass Spectrometry (LA-ICP-MS).," *J. Vis. Exp.*, no. 119, Jan. 2017, doi: 10.3791/55042.

[39] S. Theiner *et al.*, "Tumor microenvironment in focus: LA-ICP-MS bioimaging of a preclinical tumor model upon treatment with platinum(IV)-based anticancer agents.," *Metallomics*, vol. 7, no. 8, pp. 1256–1264, Aug. 2015, doi: 10.1039/c5mt00028a.

[40] T. Tm, "Current Protocols in Pharmacology," *Pharmacology*, vol. Chapter 5, no. June, pp. 1–41, 2001, doi: 10.1002/0471141755.ph0908s35.

[41] L. Martí-Bonmatí, R. Sopena, P. Bartumeus, and P. Sopena, "Multimodality imaging techniques.," *Contrast Media Mol. Imaging*, vol. 5, no. 4, pp. 180–189, 2010, doi: 10.1002/cmmi.393.

[42] S. Y. Lee, S. I. Jeon, S. Jung, I. J. Chung, and C.-H. Ahn, "Targeted multimodal imaging modalities.," *Adv. Drug Deliv. Rev.*, vol. 76, pp. 60–78, Sep. 2014, doi: 10.1016/j.addr.2014.07.009.

[43] R. Misri, "Multimodality imaging," in *Molecular Imaging Techniques: New Frontiers*, Future Science Ltd, 2013, pp. 162–176.

[44] M. Wu and J. Shu, "Multimodal Molecular Imaging: Current Status and Future Directions," *Contrast Media & Mol. Imaging*, vol. 2018, p. 1382183, 2018, doi: 10.1155/2018/1382183.

[45] P. Baldinger *et al.*, "Effects of Silexan on the serotonin-1A receptor and microstructure of the human brain: a randomized, placebo-controlled, double-blind, cross-over study with molecular and structural neuroimaging.," *Int. J. Neuropsychopharmacol.*, vol. 18, no. 4, Oct. 2014, doi: 10.1093/ijnp/pyu063.

[46] Fluigigm, "Maxpar Antibody Labeling User Guide PRD002 Rev 14," 2019. https://www.fluidigm.com/binaries/content/documents/fluidigm/resources/maxpar-antibody-labeling-user-guide-prd002rev14/maxpar-antibody-labeling-user-guide-prd002rev14/fluidigm%3Afile.

[47] B. Ellenbroek and J. Youn, "Rodent models in neuroscience research: is it a rat race?," *Dis. Model. Mech.*, vol. 9, no. 10, pp. 1079–1087, Oct. 2016, doi: 10.1242/dmm.026120.

[48] M. Hołda, W. Klimek-Piotrowska, M. Koziej, K. Tyrak, and J. Hołda, "Penetration of formaldehyde based fixatives into heart," *Folia Med. Cracov.*, vol. 4, pp. 63–70, Jan. 2017.

[49] P. Singhal, N. N. Singh, G. Sreedhar, S. Banerjee, M. Batra, and A. Garg, "Evaluation of Histomorphometric Changes in Tissue Architecture in Relation to Alteration in Fixation Protocol - An Invitro Study," *J. Clin. Diagn. Res.*, vol. 10, no. 8, pp. ZC28–ZC32, Aug. 2016, doi: 10.7860/JCDR/2016/19007.8236.

[50] M. Werner, A. Chott, A. Fabiano, and H. Battifora, "Effect of formalin tissue fixation and processing on immunohistochemistry.," *Am. J. Surg. Pathol.*, vol. 24, no. 7, pp. 1016–1019, Jul. 2000, doi: 10.1097/00000478-200007000-00014.

[51] M. Bonta, J. J. Gonzalez, C. D. Quarles, R. E. Russo, B. Hegedus, and A. Limbeck, "Elemental mapping of biological samples by the combined use of LIBS and LA-ICP-MS," *J. Anal. At. Spectrom.*, vol. 31, no. 1, pp. 252–258, 2016, doi: 10.1039/C5JA00287G.

[52] J. H. Wang, K. Wang, B. Bartling, and C.-C. Liu, "The detection of alkaline phosphatase using an electrochemical biosensor in a single-step approach," *Sensors (Basel).*, vol. 9, no. 11, pp. 8709–8721, 2009, doi: 10.3390/s91108709.

[53] R. Khazipov *et al.*, "Atlas of the Postnatal Rat Brain in Stereotaxic Coordinates," *Front. Neuroanat.*, vol. 9, p. 161, Dec. 2015, doi: 10.3389/fnana.2015.00161.

[54] S. Behuet, J. N. Cremer, M. Cremer, N. Palomero-Gallagher, K. Zilles, and K. Amunts,

"Developmental Changes of Glutamate and GABA Receptor Densities in Wistar Rats.," *Front. Neuroanat.*, vol. 13, p. 100, 2019, doi: 10.3389/fnana.2019.00100.

[55] D. Gholap, J. Verhulst, W. Ceelen, and F. Vanhaecke, "Use of pneumatic nebulization and laser ablation-inductively coupled plasma-mass spectrometry to study the distribution and bioavailability of an intraperitoneally administered Pt-containing chemotherapeutic drug.," *Anal. Bioanal. Chem.*, vol. 402, no. 6, pp. 2121–2129, Feb. 2012, doi: 10.1007/s00216-011-5654-3.

[56] M. Šala, V. S. Šelih, and J. T. van Elteren, "Gelatin gels as multi-element calibration standards in LA-ICP-MS bioimaging: fabrication of homogeneous standards and microhomogeneity testing," *Analyst*, vol. 142, no. 18, pp. 3356–3359, 2017, doi: 10.1039/C7AN01361B.

[57] E. T. Weber and R. Andrade, "Htr2a Gene and 5-HT(2A) Receptor Expression in the Cerebral Cortex Studied Using Genetically Modified Mice.," *Front. Neurosci.*, vol. 4, 2010, doi: 10.3389/fnins.2010.00036.

[58] Y. Ohno, "New Insight into the Therapeutic Role of 5-HT1A Receptors in Central Nervous System Disorders," *Cent. Nerv. Syst. Agents Med. Chem.*, vol. 10, pp. 148–157, Jun. 2010, doi: 10.2174/187152410791196341.

[59] M. Pompeiano, J. M. Palacios, and G. Mengod, "Distribution and cellular localization of mRNA coding for 5-HT1A receptor in the rat brain: correlation with receptor binding," *J. Neurosci.*, vol. 12, no. 2, pp. 440 LP – 453, Feb. 1992, doi: 10.1523/JNEUROSCI.12-02-00440.1992.

[60] E. González de San Román *et al.*, "Molecular composition of the human primary visual cortex profiled by multimodal mass spectrometry imaging," *Brain Struct. Funct.*, vol. 223, no. 6, pp. 2767–2783, 2018, doi: 10.1007/s00429-018-1660-y.

[61] M. Baker, "Reproducibility crisis: Blame it on the antibodies.," *Nature*, vol. 521, no. 7552. England, pp. 274–276, May 2015, doi: 10.1038/521274a.

[62] I. Prassas and E. P. Diamandis, "Translational researchers beware! Unreliable commercial immunoassays (ELISAs) can jeopardize your research.," *Clinical chemistry and laboratory medicine*, vol. 52, no. 6. Germany, pp. 765–766, Jun. 2014, doi: 10.1515/cclm-2013-1078.

[63] M. A. Helsby, J. R. Fenn, and A. D. Chalmers, "Reporting research antibody use: how to increase experimental reproducibility," *F1000Research*, vol. 2, p. 153, Jul. 2013, doi: 10.12688/f1000research.2-153.v2.

[64] B. Paul *et al.*, "Visualising mouse neuroanatomy and function by metal distribution using laser ablation-inductively coupled plasma-mass spectrometry imaging," *Chem. Sci.*, vol. 6, no. 10, pp. 5383–5393, Oct. 2015, doi: 10.1039/c5sc02231b.

[65] Thermo Fisher Scientific, "iCAP Q Operating Manual," 2012. https://assets.thermofisher.com/TFS-Assets/CMD/manuals/1288090-iCAP-Q-Operating-Manual-RevB.pdf.

Appendix I

Material and Methods

List of equipment

Description	Manufacturer
Analytic Balance	Sartorius
CryoStar NX50 Cryostat	ThermoFisher Scientific
Gelatine from Porcine 500g	Sigma Aldrich
Indium tin oxide coated glass slide, square	Sigma Aldrich
Microtome Blade C35	Feather
Microtube 1.5 ml	Eppendorf AG
Microtube 2.0 ml	Eppendorf AG
NWR213 Laser Ablation System	Elemental Scientific Lasers (ESI)
PIPETMAN P1000, pipette	Gilson Inc
PIPETMAN P2, pipette	Gilson Inc.
PIPETMAN P20, pipette	Gilson Inc.
PIPETMAN P200, pipette	Gilson Inc.
Reference 10, pipette	Eppendorf
Reference 100, pipette	Eppendorf
Reference 20, pipette	Eppendorf
Reference 200, pipette	Eppendorf
Replacement Glass Insert 70mm wide	Leica
Research 1000, pipette	Eppendorf
Specimen stages	Fisher Scientific
Tip FT 10 (E), pipette tips	Greiner bio-one
Tip FT 1000 (E), pipette tips	Greiner bio-one
Tip FT 20 (E), pipette tips	Greiner bio-one
Tip FT 200 (E), pipette tips	Greiner bio-one
Tissue-Plus O.C.T. Compound	Fischer Scientific

50 ml falcon tube	Eppendorf
VC-11 Handheld multimeter	Voltcraft
iCAP Q ICP-MS	Thermo Scientific
Neslab ThermoFlex 2500 Cooler	Thermo Scientific
Water cooler	New Wave Research

List of chemicals

Description	**Manufacturer**
Aceton	Merck
APES *(3-Aminopropyltriethoxysilan)*	Merck
Bond-Breaker TCEP Solution	ThermoFisher Scientific
Nitric Acid 65%	Emsure
PBS (1X)	ThermoFisher Scientific
TBS (20X)	ThermoFisher Scientific
Triton-X100	PanReac AppliChem

List of antibodies

Description	**Manufacturer**
Anti-HTR1A SAB2501759	Sigma Aldrich
Anti-HTR2A SAB4301791	Sigma Aldrich
Anti-NMDA receptor/GRIN1 SAB2500698	Sigma Aldrich

List of kits

Description	**Manufacturer**
Maxpar Antibody Labeling Kit – 141 Pr 4X	Fluidigm
Maxpar Antibody Labeling Kit – 141 Pr 40X	Fluidigm
Maxpar Antibody Labeling Kit – 151 Eu 4X	Fluidigm
Maxpar Antibody Labeling Kit – 151 Eu 40X	Fluidigm
Maxpar Antibody Labeling Kit – 171Yb 40X	Fluidigm

Appendix II

Protocol for lanthanide labelling of antibodies

The following original protocol by Fluidigm was adapted and used for conjugation [46]. Adaptations are mentioned in section "Methods".

0:00 Preload the polymer with lanthanide.

1. Spin the polymer tube for 10 seconds in a microfuge to ensure that the reagent is at the bottom of the tube.

2. Resuspend the polymer with 95 µL of L-Buffer.

3. Mix thoroughly by pipetting.

4. Add 5 µL of lanthanide metal solution to the tube (final concentration: 2.5 mM in 100 µL).

5. Mix thoroughly by pipetting.

6. Incubate at 37 °C for 30−40 minutes in a water bath. During incubation, proceed immediately to Step 7 and begin buffer exchange and partial reduction of antibody.

0:30 Perform buffer exchange and partially reduce the antibody

7. Add 100 µg of stock antibody in up to 400 µL R-Buffer to a 50 kDa filter.

8. Centrifuge at 12,000 x g for 10 minutes at room temperature.

9. During centrifugation, dilute 0.5 M TCEP stock to 4 mM in R-Buffer by mixing 8 µL of 0.5 M TCEP stock with 992 µL of R-Buffer. For each antibody being labelled, 100 µL of 4 mM TCEP-R-Buffer is required.

10. Discard column flow-through from centrifugation.

11. Add 100 µL of the 4 mM TCEP-R-Buffer to each antibody and mix by pipetting.

12. Incubate at 37 °C in a water bath for 30 minutes. Proceed to Step 13 during the 30-minute incubation.

IMPORTANT: Do not exceed 30 minutes! Proceed immediately to Step 17 after 30 minutes and begin purifying the partially reduced antibody.

0:45 Purify the lanthanide-loaded polymer

NOTE: Purify the lanthanide-loaded polymer at the same time that the antibody is being reduced (Step 12)

13. Add 200 µL of L-Buffer to a 3 kDa filter.

14. Add the 100 µL metal-loaded polymer mixture to the filter containing the 200 µL L-Buffer to the wash.

15. Centrifuge at 12,000 x g for 25 minutes at room temperature.

16. Repeat the wash by adding 400 µL of C-Buffer to the filter and centrifuge at 12,000 x g for 30 minutes at room temperature.

1:15 Purify the partially reduced antibody.

17. Retrieve the 50 kDa filter containing the partially reduced antibody from the 37 °C water bath.

18. Add 300 µL of C-Buffer to the 50 kDa filter to wash the antibody.

19. Centrifuge at 12,000 x g for 10 minutes at room temperature.

20. Discard flow-through.

21. Repeat the wash by adding 400 µL of C-Buffer to the filter and centrifuge at 12,000 x g for 10 minutes at room temperature.

1:40 Retrieve the purified partially reduced antibody and lanthanide-loaded polymer

22. Retrieve 3 kDa filter containing the purified lanthanide-loaded polymer from the centrifuge and discard column flow-through.

23. Retrieve 50 kDa filter containing the purified partially reduced antibody from the centrifuge and discard column flow-through.

1:45 Conjugate the antibody with lanthanide-loaded polymer.

24. Using a pipette, resuspend the lanthanide-loaded polymer in 60 µL of C-Buffer (total volume ~80 µL).

25. Transfer the resuspended contents to the corresponding partially reduced antibody in the 50 kDa filter (final conjugation volume ~100 µL).

26. Mix gently by pipetting.

27. Incubate at 37 °C for 90 minutes.

3:15 Wash the metal-conjugated antibody.

28. Add 200 µL of W-Buffer to the 100 µL antibody conjugation mixture.

29. Centrifuge at 12,000 x g for 10 minutes.

30. Discard flow-through.

31. Repeat wash three more times with W-Buffer up to a total volume of 400 µL (for a total of four washes with W-Buffer).

4:00 Determine yield

32. After the final wash with W-buffer, add ~80 µL of W-buffer to the 50 kDa filter to dilute the conjugate (in ~20 µL) to a volume of 100 µL. Pipette to mix and rinse the walls of the filter.

33. Quantify the conjugated antibody by measuring the absorbance at 280 nm against a W-Buffer blank (expected recovery is 60%).

34. Calculate the volume of antibody stabilization buffer (supplemented with 0.05% sodium azide after purchase) required to obtain a final concentration of 0.5 mg/mL.

35. Centrifuge the 50 kDa filter at 12,000 x *g* for 10 minutes to remove the W-Buffer.

4:20 Recover and store the metal-conjugated antibody.

36. Add the calculated volume of antibody stabilization buffer (120 µL, for about 60% recovery of the antibody) minus the residual volume (~20 µL) to the 50 kDa filter to obtain a final concentration of 0.5 mg/mL of conjugated antibody.

37. Invert the 50 kDa filter over to a new collection tube.

38. Centrifuge the inverted filter/collection tube assembly at 1,000 x g for 2 minutes.

39. Store at 4 °C.

40. Titrate the antibody. We recommend titrating the antibody with relevant positive and negative controls for the experimental system in which the antibody will be used. Set up the titration as follows: 5 µg/mL, 2.5 µg/mL, 1.25 µg/mL, 0.62 µg/mL, 0.31 µg/mL, 0.16 µg/mL, 0 µg/mL.

41. After the conjugated antibody has been titrated on the CyTOF® instrument, if necessary dilute it to the optimum working concentration in stabilization buffer and store it at 4 °C.

Immunohistochemical protocols

Protocols regarding fixation

-80° C → -20° C for 20-30´ → 4°C for 5-10´

Fixation in 4°C acetone for 10´

Let acetone evaporate

Blocking with 3% BSA 45´

Incubation o/n 4°C in hydration chamber or 1h at RT

Washing step with 1x TBS with 0,2%Triton-X for 2´

Washing step with 1x TBS for 2x2´

Air dry 20´ at RT in laminar flow hood

-80° C → -20° C for 20-30´ → 4°C for 5-10´

Fixation in 4°C 4% PFA for 30´

Washing step 3x5´ in 1xTBS at RT

Blocking with 3% BSA 45´

Incubation o/n 4°C in hydration chamber or 1h at RT

Washing step with 1x TBS with 0,2%Triton-X for 2´

Washing step with 1x TBS for 2x2´

Air dry 20´ at RT in laminar flow hood

Protocols regarding tissue drying

-80° C → -20° C for 20-30´ → 4°C for 5-10´

Fixation in 4°C acetone for 10´

Let acetone evaporate

Blocking with 3% BSA 45´

Incubation o/n 4°C in hydration chamber or 1h at RT

Washing step with 1x TBS with 0,2%Triton-X for 2´

Washing step with 1x TBS for 2x2´

Air dry 20´ at RT in laminar flow hood

-80° C → -20° C for 20-30´ → 4°C for 5-10´

Fixation in 4°C acetone for 10´

Let acetone evaporate

Blocking with 3% BSA 45´

Incubation o/n 4°C in hydration chamber or 1h at RT

Washing step with 1x TBS with 0,2%Triton-X for 2´

Washing step with 1x TBS for 2x2´

Air dry 20´ in desiccator

Protocols regarding blocking

-80° C → -20° C for 20-30´ → 4°C for 5-10´

Fixation in 4°C acetone for 10´

Let acetone evaporate

Blocking with 3% BSA 45´

Incubation o/n 4°C in hydration chamber or 1h at RT

Washing step with 1x TBS with 0,2%Triton-X for 2´

Washing step with 1x TBS for 2x2´

Air dry 20´ at RT in laminar flow hood

-80° C → -20° C for 20-30´ → 4°C for 5-10´

Fixation in 4°C acetone for 10´

Let acetone evaporate

Blocking with 10% goat serum 45´

Incubation o/n 4°C in hydration chamber or 1h at RT

Washing step with 1x TBS with 0,2%Triton-X for 2´

Washing step with 1x TBS for 2x2´

Air dry 20´ at RT in laminar flow hood

-80° C → -20° C for 20-30´ → 4°C for 5-10´

Fixation in 4°C acetone for 10´

Let acetone evaporate

Blocking with 3% BSA and10% goat serum 45´

Incubation o/n 4°C in hydration chamber or 1h at RT

Washing step with 1x TBS with 0,2%Triton-X for 2´

Washing step with 1x TBS for 2x2´

Air dry 20´ at RT in laminar flow hood

Protocols regarding detergent

-80° C → -20° C for 20-30´ → 4°C for 5-10´

Fixation in 4°C acetone for 10´

Let acetone evaporate

Blocking with 3% BSA 45´

Incubation o/n 4°C in hydration chamber or 1h at RT

Washing step with 1x TBS with 0,2%Triton-X for 2´

Washing step with 1x TBS for 2x2´

Air dry 20´ at RT in laminar flow hood

-80° C → -20° C for 20-30´ → 4°C for 5-10´

Fixation in 4°C acetone for 10´

Let acetone evaporate

Blocking with 3% BSA 45´

Incubation o/n 4°C in hydration chamber or 1h at RT

Washing step with 1x TBS with 0,025%Triton-X for 2´

Washing step with 1x TBS for 2x2´

Air dry 20´ at RT in laminar flow hood

I have tried to find all owners of the image rights and obtained their consent to the use of the images in this work. Should a copyright infringement become known, I request that you notify me.

Appendix III

Figures

Tables